



# Blended particle methods with adaptive subspaces for filtering turbulent dynamical systems



Di Qi\*, Andrew J. Majda

Department of Mathematics and Center for Atmosphere and Ocean Science, Courant Institute of Mathematical Sciences, New York University, New York, NY 10012, United States

## HIGHLIGHTS

- We develop blended filtering methods that exploit the structure of dynamical systems.
- Non-Gaussian features are captured adaptively in a subspace through particle methods.
- The remaining parts of the phase space are amended by conditional Gaussian mixtures.
- The performance of the blended algorithms is compared in various dynamical regimes.

## ARTICLE INFO

### Article history:

Received 1 November 2014  
 Received in revised form  
 1 February 2015  
 Accepted 4 February 2015  
 Available online 11 February 2015  
 Communicated by T. Wanner

### Keywords:

Data assimilation  
 Hybrid filters  
 Curse of dimensionality  
 Turbulent dynamical systems

## ABSTRACT

It is a major challenge throughout science and engineering to improve uncertain model predictions by utilizing noisy data sets from nature. Hybrid methods combining the advantages of traditional particle filters and the Kalman filter offer a promising direction for filtering or data assimilation in high dimensional turbulent dynamical systems. In this paper, blended particle filtering methods that exploit the physical structure of turbulent dynamical systems are developed. Non-Gaussian features of the dynamical system are captured adaptively in an evolving-in-time low dimensional subspace through particle methods, while at the same time statistics in the remaining portion of the phase space are amended by conditional Gaussian mixtures interacting with the particles. The importance of both using the adaptively evolving subspace and introducing conditional Gaussian statistics in the orthogonal part is illustrated here by simple examples. For practical implementation of the algorithms, finding the most probable distributions that characterize the statistics in the phase space as well as effective resampling strategies is discussed to handle realizability and stability issues. To test the performance of the blended algorithms, the forty dimensional Lorenz 96 system is utilized with a five dimensional subspace to run particles. The filters are tested extensively in various turbulent regimes with distinct statistics and with changing observation time frequency and both dense and sparse spatial observations. In real applications perfect dynamical models are always inaccessible considering the complexities in both modeling and computation of high dimensional turbulent system. The effects of model errors from imperfect modeling of the systems are also checked for these methods. The blended methods show uniformly high skill in both capturing non-Gaussian statistics and achieving accurate filtering results in various dynamical regimes with and without model errors.

© 2015 Elsevier B.V. All rights reserved.

## 1. Introduction

Accurate predictions of the future states of high-dimensional turbulent dynamical systems are a formidable problem with significant practical impact in a wide range of areas throughout

science and engineering. Filtering or data assimilation refers to the process of obtaining the best estimation of a natural system by combining uncertain model predictions with noisy observations of the true signal from nature. Examples for important contemporary applications involve the real time filtering and prediction of weather and climate systems as well as the spread of hazardous plumes and pollutants or the prediction of storm surges in environmental science and engineering. These turbulent dynamical systems always include a large number of active degrees of freedom under various kinds of nonlinear non-Gaussian

\* Corresponding author.

E-mail address: [qidi@cims.nyu.edu](mailto:qidi@cims.nyu.edu) (D. Qi).

scenarios even with an irreducible high dimensional attractor in phase space. Considering the complexity of these systems, model errors in the approximation models are always unavoidable due to both the imperfect understanding of the real nature systems and the limited computational ability at hand. Thus an important emerging scientific issue is the development of statistically accurate filtering methods through models with high skill in capturing both Gaussian and non-Gaussian features as well as being robust to external perturbations and imperfect prior estimates from model errors for filtering turbulent dynamical systems.

The complexity of the turbulent dynamical systems makes it impossible to evaluate the distributions of state variables analytically in explicit form for most situations. To approximate the filter distributions computationally instead, particle filters based on Monte-Carlo simulations are a popular class of numerical methods in characterizing the nonlinear non-Gaussian structures of low-dimensional systems [1,2]. Compared with the standard Kalman filtering methods [3], the principal advantage of the particle methods is that they do not rely on any local linearization of the models and in principle can get the entire statistical information about any higher order moments with large enough ensemble size. However the price that must be paid for these advantages of higher accuracy is the high computational expense required to evolve and update the entire ensemble of particles. Especially, as the dimensionality of the system increases, the required ensemble size that is sufficient for describing the full statistics in the phase space increases exponentially and becomes computationally impossible even with moderate dimensionality about order of 100. Insufficient ensemble size will end up with frequent particle collapse even with proper resampling strategies [4,5].

To avoid this curse of dimensionality for particle methods, a number of ensemble based Kalman filters [6–9] are developed, which use an ensemble of particles to estimate the mean and covariance only and then apply Kalman filter instead in the analysis step. These ensemble Kalman filtering methods show promising results for some high dimensional nonlinear systems, for example in synoptic scale midlatitude weather dynamics, with careful choices of inflation and localization parameters for the particles. But still with only Gaussian statistics of the particles exploited in the analysis step, these methods are implicitly Gaussian and are sensitive to model resolution and different kinds of observations, and model parameters need to be changed according to different dynamical regimes. For another direction, reduced order filtering strategies [10–13] and Bayesian hierarchical modeling methods [14] have been developed trying to apply particles in a sufficiently low dimensional subspace. One idea might be that only considering the subspace which contains most of the energy in the system is sufficient to obtain desirable filtering performance. One strategy related to this idea is to filter the solution in an evolving low-dimensional subspace which captures the leading variances adaptively while ignoring the remaining degrees of freedom [15]. Whereas it turned out that the ignored degrees of freedom could be crucial in the model prediction skills. Simple examples with non-normal linear systems [16] demonstrate the limited skill of such an approach for reduced filtering methods in general as shown here in Section 2.2.1. Despite the difficulties in both the Kalman filter based Gaussian methods and the reduced order particle strategies, these two approaches with distinct features both have some advantages in achieving promising filtering performance and are often complementary with each other. Ideas about hybrid methods [17,18] have been developed and show promising results.

This paper builds on the mathematical framework described in [19] to develop new blended particle filtering methods for chaotic dynamical systems. The idea is a hybrid method combining the merits of the adaptive reduced order method as well as conditional Gaussian mixtures in which Kalman filter update formulas can be

applied in the analysis step. The large dimensional phase space is decomposed into two subspaces. The particle filter is applied in one subspace low dimensional enough for accuracy and efficiency and evolving adaptively in time for capturing the directions with principal variances. On the other hand, the information in the high dimensional orthogonal subspace is corrected by a conditional Gaussian mixture representation where Kalman filter updates can be used with efficiency. The adaptive space decomposition required in this framework for the forecast model is achieved here with the help of recently developed statistically accurate models [16,20,21] in this paper, while the general framework is more flexible and need not be limited to these forecast models only. See [22,23] for another application of the blended filtering ideas using multi-scale forecast models with superparameterization. Two essential aspects concerning different statistics in the two separate subspaces are highlighted here for the effectiveness of this method. The low dimensional subspace with particle filters used to resolve full statistics needs to evolve adaptively in time in order to keep tracking the most energetic directions of the system with largest variances; while the statistics in the orthogonal subspace with conditional Gaussian mixtures applied are nevertheless important and should never be neglected. The importance of these two aspects can be illustrated by simple test models. The choice for the Gaussian distributions in the orthogonal subspace is guided by information theory and can be approximated by solving a linear system conditional on particle values in the other subspace. The efficiency of the method is guaranteed by a universal form of the prior conditional covariance matrix to which the Kalman filter update is applied, requiring only one time calculation of the large scale Kalman gain matrix. In addition, to avoid particle degeneration while maintaining the minimum amount of noise added in the resampling step, an adaptive inflation is introduced to the resampled particles which has potential to further stabilize the scheme. In [19], we have checked the blended filters in several difficult regimes using the Lorenz-96 system with no model error included. Here, a more extensive discussion about the performances of these methods is carried out in both Gaussian and non-Gaussian regimes of the same system with various kinds of observation networks. Furthermore, the effects of model error are checked by introducing imperfect external forcing term in this system. It could make the problem much more challenging due to the distinct statistical dynamics between the perfect model and the imperfect model with error. The ability of these methods to capture significant non-Gaussian features with imperfect model is demonstrated below in Section 4.

In the following part of this paper, in Section 2, the general ideas and basic framework for the blended particle filtering algorithms will be described. We illustrate the importance of the two indispensable parts of this method with several simple examples in Section 2. Section 3 describes the detailed strategies for finding the conditional Gaussian distribution and the resampling tricks, which are essential to the realizability and stability of these hybrid filtering schemes. Various tests of these methods using the Lorenz-96 system are reported in Section 4 for models with or without model errors including the capability of the methods to capture non-Gaussian features. We finish in Section 5 with a brief summary and a discussion about the future directions.

## 2. Algorithms for blended particle filtering

The blended particle filtering algorithms exploit the physical structure of turbulent dynamical systems and capture non-Gaussian features in an adaptively evolving low dimensional subspace through particles interacting with evolving Gaussian statistics on the remaining portion of phase space. This framework is set to be flexible so that any proper forecast models with

blended reduced order subspaces or multi-scale structure can be incorporated. Another application of these ideas for multiscale filtering algorithms can be found in [23,22]. As shown in the following subsections, the algorithms consist of two indispensable parts: (i) an adaptively evolving subspace capturing the principal directions of the system; (ii) a conditional Gaussian mixture representation in the high-dimensional orthogonal subspace. To illustrate the importance of these two features, a simple  $2 \times 2$  non-normal linear system and then the more complex Lorenz-96 system will be applied to emphasize that ignoring either of these two essential parts will end up with large filtering error or even filter divergence.

### 2.1. General framework for the blended particle filtering methods

Here we consider real time filtering or data assimilation algorithms for a state vector  $\mathbf{u}(t) \in \mathbb{R}^N$ , evaluated at discrete time steps  $t \in \mathbb{N}^+$ , from a turbulent dynamical system. The aim is to estimate the state variables recursively in time by a *posterior distribution* denoted as  $p_+(\mathbf{u}_t) \equiv p(\mathbf{u}_t|\mathbf{v}_{1:t})$ , by combining the information from model forecasts and the observations  $\mathbf{v} \in \mathbb{R}^M$ ,  $M \leq N$ , up to time  $t$ . Generally this process can be achieved by two recursive steps. At one time instant  $t$ , first some Markov prediction model for the dynamical system with transition equation  $p(\mathbf{u}_t|\mathbf{u}_{t-1})$  is used to get the *prior distribution*

$$p_-(\mathbf{u}_t) \equiv p(\mathbf{u}_t|\mathbf{v}_{1:t-1}) = \int p(\mathbf{u}_t|\mathbf{u}_{t-1})p(\mathbf{u}_{t-1}|\mathbf{v}_{1:t-1})d\mathbf{u}_{t-1}; \quad (1)$$

second, the posterior distribution is achieved by incorporating the observation data with the model forecasts with the help of the Bayesian formula

$$p_+(\mathbf{u}_t) \equiv p(\mathbf{u}_t|\mathbf{v}_{1:t}) = \frac{p(\mathbf{v}_{1:t}|\mathbf{u}_t)p_-(\mathbf{u}_t)}{\int p(\mathbf{v}_{1:t}|\mathbf{u}_t)p_-(\mathbf{u}_t)d\mathbf{u}_t}. \quad (2)$$

In the case of filtering high dimensional turbulent dynamical systems, challenges exist in both the forecast step (1) and the analysis step (2). In the forecast part, the task is to find a proper uncertainty quantification (UQ) method to estimate the transition equation for  $p(\mathbf{u}_t|\mathbf{u}_{t-1})$ . It is always computational forbidden to fully resolve all the degrees of freedom of the system whereas high order statistics could play crucial roles for systems with nonlinearities in accurate prediction of the state variables. Thus it is reasonable to seek ideas about reduced order blended methods considering two separate subspaces with important higher order statistics captured fully in a low dimensional subspace with efficiency. With the model predictions in two separate subspaces achieved, the difficulty in the analysis step is to find a statistically consistent way to incorporate the observation data, which in general is a mixture of the two subspaces, into the model prior forecasts so different filtering strategies can be applied to these two subspaces considering their different statistical structure. First the mathematical foundations for blending model forecasts and observation data in the analysis step will be described, then several effective prediction models developed recently [16,20,21] will be proposed to be applied to the mathematical framework as the forecast models. For simplicity in representation, we will neglect the subscript  $t$  in the remainder of the paper.

#### 2.1.1. Analysis step

For the blended methods, the state variable  $\mathbf{u}$  is decomposed into two adaptively evolving subspaces  $\mathbf{u} = (\mathbf{u}_1, \mathbf{u}_2)$ ,  $\mathbf{u}_j \in \mathbb{R}^{N_j}$ ,  $N_1 + N_2 = N$ , with the property that  $N_1$  is low dimensional enough so that the statistics of  $\mathbf{u}_1$  can be calculated from a particle filter while the statistics of  $\mathbf{u}_2$  are assumed to be conditional Gaussian given  $\mathbf{u}_1$ . The  $\mathbf{u}_1$  subspace is then described by an ensemble

of particles with values and weights in  $\{\mathbf{u}_{1,j}, p_j\}$ , and the  $\mathbf{u}_2$  subspace is described by a Gaussian mixture distribution  $\mathcal{N}(\bar{\mathbf{u}}_{2,j}, R_{2,j})$  with mean and covariance matrix conditional on the values in  $\mathbf{u}_1$  subspace (one practical way to estimate the conditional mean and covariance will be discussed in the next section). Therefore given a proper forecast model and the decomposition described above, the prior forecast density at any analysis time step  $m\Delta t$  is given by

$$p_-(\mathbf{u}) = p_-(\mathbf{u}_1)p_-^G(\mathbf{u}_2|\mathbf{u}_1) = \sum_{j=1}^Q p_{j,-} \delta(\mathbf{u}_1 - \mathbf{u}_{1,j}) \mathcal{N}(\mathbf{u}_2|\bar{\mathbf{u}}_{2,j}^-, R_{2,j}^-), \quad (3)$$

where the marginal distribution  $p_-(\mathbf{u}_1)$  is approximated by  $Q$ -particles with importance weight,  $p_{j,-}$ , while the distribution in the orthogonal subspace  $p_-^G(\mathbf{u}_2|\mathbf{u}_1)$  is assumed to be Gaussian given values of  $\mathbf{u}_1$  (one derivation using information theory and max-entropy principle is demonstrated in the next section showing this Gaussian assumption about the variables in the  $\mathbf{u}_2$  subspace is appropriate). Introduce observations at the analysis time,  $m\Delta t$ , in the form

$$\mathbf{v} = G(\mathbf{u}) + \sigma_0 = G_0(\mathbf{u}_1) + G_1(\mathbf{u}_1)\mathbf{u}_2 + \sigma_0, \quad (4)$$

where  $G_1(\mathbf{u}_1)$  has rank  $M$  and the observation noise,  $\sigma_0$ , is Gaussian  $\sigma_0 \sim \mathcal{N}(\mathbf{0}, R_0)$ . This can be viewed as a first order expansion of the mixed observation operator  $G(\mathbf{u}_1, \mathbf{u}_2)$  around the value of  $\mathbf{u}_1$  and of course, any linear observation operator has this form.

The task now is to find a way to filter the variables  $\mathbf{u}_1, \mathbf{u}_2$  separately in the two subspaces due to their different representations. Given each particle value  $\mathbf{u}_{1,j}$  in the  $\mathbf{u}_1$  subspace, we can define new observations conditional on each particle value as  $\mathbf{v}'_{2,j} = G_1(\mathbf{u}_{1,j})\mathbf{u}_2 + \sigma_0$ , with  $\mathbf{v}'_{2,j} = \mathbf{v} - G_0(\mathbf{u}_{1,j})$ . Since we have Gaussian observation noise  $\sigma_0$  and conditional Gaussian distribution for  $\mathbf{u}_2$  in the subspace, a Kalman filter update can be applied for variables  $\mathbf{u}_2$  with corresponding observations  $\mathbf{v}'_2$  by using Bayesian formula in this subspace. On the other hand for variables  $\mathbf{u}_{1,j}$  with particle representations in the  $\mathbf{u}_1$  subspace, it is natural to apply particle filter to them. But a new likelihood function restrained in the  $\mathbf{u}_1$  subspace should be calculated to get the weight updating factor  $l_j$  for each particle weight  $p_j$ . In fact, by combining (3) and (4) into the analysis step equation (2) it can be shown by applying the Bayesian formula that the posterior distribution after the analysis step is also a blended particle filter conditional Gaussian distribution [19, see], i.e. there are explicit formulas for the updated weights,  $p_{j,+}$ ,  $1 \leq j \leq Q$ , conditional mean,  $\bar{\mathbf{u}}_{2,j}^+$ , and covariance,  $R_{2,j}^+$ , so that

$$p_+(\mathbf{u}) = \sum_{j=1}^Q p_{j,+} \delta(\mathbf{u}_1 - \mathbf{u}_{1,j}) \mathcal{N}(\mathbf{u}_2|\bar{\mathbf{u}}_{2,j}^+, R_{2,j}^+). \quad (5)$$

Below, we will use ‘-’ to represent prior values and ‘+’ for posterior values. The posterior particle weights can be updated as  $p_{j,+} \propto p_{j,-} l_j$ , with  $l_j \propto \int p(\mathbf{v}|\mathbf{u}_{1,j}, \mathbf{u}_2) \mathcal{N}(\mathbf{u}_2|\bar{\mathbf{u}}_{2,j}^-, R_{2,j}^-) d\mathbf{u}_2$  measuring the accuracy of the particle values in the subspace by comparing with the observations, which can be expressed in an explicit form with Gaussian noise in observation. The posterior distributions  $\mathcal{N}(\mathbf{u}_2|\bar{\mathbf{u}}_{2,j}^+, R_{2,j}^+)$  in the orthogonal subspace are updated by suitable Kalman filter formulas with the mean update for  $\bar{\mathbf{u}}_{2,j}^+$  depending nonlinearly on  $\mathbf{u}_{1,j}$  in general (check the explicit formulas for both particle filter and Kalman filter in the algorithm below). The details of this derivation and explicit formulas can be found in [19].

Specifically, by choosing proper blended forecast model satisfying the requirements in (3), after the forecast step, we get the predicted values for the mean states  $\bar{\mathbf{u}}$  and the full state covariance matrix  $R$ , together with a particle representation in the

low dimensional subspace  $\mathbf{u}_1$  through dynamical basis  $E(t) = \{\mathbf{e}_1(t), \dots, \mathbf{e}_s(t)\}$  evolving in time, with dimensionality  $s = N_1 \ll N$ ,

$$\mathbf{u}(t) = \bar{\mathbf{u}}(t) + \sum_{j=1}^s u'_{1,j}(t; \omega) \mathbf{e}_j(t), \quad (6)$$

where  $\{\mathbf{e}_j(t)\}_{j=1}^s$  is the subdimensional dynamical basis, and  $\{u'_{1,j}\}$  are the corresponding stochastic coefficients computed through Monte-Carlo simulation. The particle statistics represented by the statistical coefficients  $u'_{1,j}$  must be consistent with the covariance matrix  $R$ , and  $u'_{1,i}, u'_{1,j}$  are normalized to be independent with each other, that is

$$\langle u'_{1,i} u'^*_{1,j} \rangle = \mathbf{e}_i \cdot R \mathbf{e}_j \delta_{ij}, \quad 1 \leq i, j \leq s.$$

In the following analysis step, define the projection operator  $PP^T$  calculated by completing the dynamical basis  $P = [E, E^\perp]$ , and project the mean and covariance to the two subspaces spanned by  $E$  and  $E^\perp$ . At the initial time,  $t = 0$ , each particle is equally weighted as  $(u'_{1,i}, p_i) = (u'_{1,i}, \frac{1}{Q})$ . The general algorithm for the analysis step is sketched in two parts.

**Algorithm. Blended filtering method (analysis step)**

• Part I

- Project the forecast mean and covariance matrix to the two subspaces

$$\begin{pmatrix} \bar{\mathbf{u}}_1^- \\ \bar{\mathbf{u}}_2^- \end{pmatrix} = P^T \bar{\mathbf{u}}^-, \quad R_t = P^T R P = \begin{pmatrix} R_1 & R_{12} \\ R_{12}^T & R_2 \end{pmatrix}. \quad (7)$$

- Calculate the conditional mean  $\bar{\mathbf{u}}_{2,j}^-$ , consistent with the mean  $\bar{\mathbf{u}}_2^-$  and cross-covariance  $R_{12}$ , in the orthogonal subspace  $p_{2,j}^- (\mathbf{u}_2 | \mathbf{u}_1, j) = \mathcal{N}(\bar{\mathbf{u}}_{2,j}^-, R_2^-)$  with dependence on the values of the particles  $\mathbf{u}_{1,j}$ .
- Calculate the conditional covariance  $R_2^-$  in the  $\mathbf{u}_2$  subspace determined by subtracting the variances of the conditional mean  $\bar{\mathbf{u}}_{2,j}^-$  from the original prior covariance matrix  $R_2$  (denote  $\mathbf{u}'_1 = \mathbf{u}_1 - \langle \mathbf{u}_1 \rangle$ ,  $\bar{\mathbf{u}}'_2(\mathbf{u}_1) = \bar{\mathbf{u}}_2(\mathbf{u}_1) - \langle \mathbf{u}_2 \rangle$  as the fluctuations about the mean, and details about this correction will be discussed in the next section):

$$R_2^- = R_2 - \sum_j \bar{\mathbf{u}}'_{2,j} \otimes \bar{\mathbf{u}}'_{2,j} p_{j,-}. \quad (8)$$

• Part II

- Use Kalman filter updates in the  $\mathbf{u}_2$  subspace

$$\bar{\mathbf{u}}_{2,j}^+ = \bar{\mathbf{u}}_{2,j}^- + K (\mathbf{v} - G E \mathbf{u}_{1,j}^- - G E^\perp \bar{\mathbf{u}}_{2,j}^-), \quad (9a)$$

$$\tilde{R}_2^+ = (I - K G E^\perp) R_2^-, \quad (9b)$$

$$K = R_2^- (G E^\perp)^T (G E^\perp R_2^- (G E^\perp)^T + R_0)^{-1}, \quad (9c)$$

with the (linear) observation operator  $G(\mathbf{u}_1, \mathbf{u}_2) = G E \mathbf{u}_1 + G E^\perp \mathbf{u}_2$ , where  $R_0$  is the covariance matrix for the observation noise.

- Update the particle weights in the  $\mathbf{u}_1$  subspace by  $p_{j,+} \propto p_{j,-} l_j$ , with

$$l_j = \exp \left[ \frac{1}{2} \left( \bar{\mathbf{u}}_{2,j}^{+T} R_2^{+^{-1}} \bar{\mathbf{u}}_{2,j}^+ - \bar{\mathbf{u}}_{2,j}^{-T} R_2^{-^{-1}} \bar{\mathbf{u}}_{2,j}^- - (\mathbf{v} - G E \mathbf{u}_{1,j}^-)^T R_0^{-1} (\mathbf{v} - G E \mathbf{u}_{1,j}^-) \right) \right]. \quad (10)$$

- Normalize the weights  $p_{j,+} = \frac{p_{j,-} l_j}{\sum_j p_{j,-} l_j}$  and apply resampling.
- Get the posterior mean and covariance matrix from the posterior particle presentation

$$\bar{\mathbf{u}}_1^+ = \sum_j \mathbf{u}_{1,j} p_{j,+}, \quad \bar{\mathbf{u}}_2^+ = \sum_j \bar{\mathbf{u}}_{2,j}^+ p_{j,+}, \quad (11a)$$

and

$$R_{1,ij}^+ = \sum_k u'_{1,i,k} u'^*_{1,j,k} p_{k,+}, \quad 1 \leq i, j \leq s, \quad (11b)$$

$$R_{12,ij}^+ = \sum_k u'_{1,i,k} \bar{\mathbf{u}}_{2,j,k}^{+*} p_{k,+}, \quad 1 \leq i \leq s, s+1 \leq j \leq N, \quad (11c)$$

$$R_2^+ = \tilde{R}_2^+ + \sum_j \bar{\mathbf{u}}_{2,j}^+ \otimes \bar{\mathbf{u}}_{2,j}^{+*} p_{j,+}. \quad (11d)$$

- Rotate the stochastic coefficients and basis to principal directions in the  $s$ -dimensional stochastic subspace.

**Remark.** In the algorithm above, part I serves as the pre-calculations for the predicted prior variables in the two subspaces. Note that the particle values in the  $\mathbf{u}_1$  subspace can be simply achieved through a Monte-Carlo simulation for the stochastic coefficients under the basis, whereas the conditional Gaussian mean and covariance matrix in the orthogonal  $\mathbf{u}_2$  subspace must be chosen to be consistent with the prior mean and cross-covariance  $\bar{\mathbf{u}}_2^-, R_{12}$ . We will discuss the principle in getting this conditional mean and covariance in detail in Section 3. Part II of the algorithm carries out filtering methods (particle filter in  $\mathbf{u}_1$  and Kalman filter update in  $\mathbf{u}_2$ ) separately in the two subspaces and combines them together in the end to get the initial values for next time step. Since the particle filter is only carried out in a low-dimensional reduced order subspace  $\mathbf{u}_1$ , the computational cost can be controlled and high order statistics are obtained inside this subspace. On the other hand, the orthogonal subspace  $\mathbf{u}_2$  is represented by a set of Gaussian mixtures where all the conditional means  $\bar{\mathbf{u}}_{2,j}$  share the same conditional covariance  $R_2^-$  in (8). Thus only one Kalman gain matrix  $K$  as in (9c) needs to be calculated to update mean and covariance via Kalman filter in the high dimensional orthogonal subspace. In this way, the computational cost in  $\mathbf{u}_2$  subspace is also affordable at least for moderate size turbulent dynamical systems with order of hundreds of degrees of freedom.

It also needs to be mentioned that the formulation described above is similar to the Rao-Blackwellisation for sequential importance sampling described in [24,2]. Previous formulations of the hybrid ideas with Gaussian mixtures include [17,18,25]. However, there is a crucial difference that here conditional Gaussian mixtures are applied in the reduced subspace  $\mathbf{u}_2$  blended with particle filter approximations only in the lower-dimensional subspace,  $\mathbf{u}_1$ , unlike the previous work. A realizable efficient way to marginalize the state variables into two subspaces and for judicious quantification for the uncertainties in each subspace as well as proper resampling strategies to avoid particle collapse are crucial for filter performance. These issues will be extensively discussed in the following sections.

### 2.1.2. Forecast step

The framework of the algorithm described above leaves us with extra freedom to choose from admissible forecast models and proper space decomposition strategies, which makes the scheme quite flexible to be hybridized with various other methods. While the above formulation can be applied to hybrid particle filters with conditional Kalman filters on fixed subspaces, a more attractive idea is to utilize statistical forecast models that adaptively change these subspaces as time evolves in response to the uncertainty without a separation of time scales. Among the favorable choices of forecast models, there include the nonlinear statistical dynamical models (QG-DO or MQG-DO) developed recently in [16,20,21] which have been proved to have significant skill for uncertainty quantification for turbulent dynamical systems. Here we describe the ideas in these methods briefly using the abstract form of turbulent dynamical systems with quadratic nonlinearity

$$\mathbf{u}_t = L \mathbf{u} + \mathbf{B}(\mathbf{u}, \mathbf{u}) + \mathbf{F}, \quad (12)$$

where  $\mathbf{B}(\mathbf{u}, \mathbf{u})$  represents quadratic nonlinear interactions which conserves energy  $\mathbf{u} \cdot \mathbf{B}(\mathbf{u}, \mathbf{u}) = 0$ . The structure (12) for turbulent dynamical systems can be found in many applications in geosciences and other areas [26–29].

The idea for solving this system is to derive statistically accurate closed forms for the dynamics of each order of moments (most importantly, the mean and covariance matrix) for the state variables  $\mathbf{u}$ . Taking the same decomposition of state variables into mean and fluctuation sums as in (6) in a  $s$ -dimensional phase space  $V_s = \text{span}\{\mathbf{e}_1, \mathbf{e}_2, \dots, \mathbf{e}_s\}$  (with  $s = N$  as the fully spatial decomposition and  $s < N$  as the reduced order decomposition in a subspace),

$$\mathbf{u}(t) = \bar{\mathbf{u}}(t) + \sum_{j=1}^s u'_j(t; \omega) \mathbf{e}_j(t),$$

the dynamical equations for the mean  $\bar{\mathbf{u}}$  and covariance matrix  $R_{ij} = \langle u'_i u'^*_j \rangle$  can be derived by substituting the decomposition into the original system (12) and taking expectations for the corresponding parts, therefore

$$\frac{d\bar{\mathbf{u}}}{dt} = L\bar{\mathbf{u}} + \mathbf{B}(\bar{\mathbf{u}}, \bar{\mathbf{u}}) + \sum_{i,j} R_{ij} \mathbf{B}(\mathbf{e}_i, \mathbf{e}_j) + \mathbf{F}, \quad (13a)$$

$$\frac{dR}{dt} = L_v R + R L_v^* + Q_F. \quad (13b)$$

It can be noticed that the dynamics for the mean (13a) is related with the second order moments  $R$ , and the dynamics for the covariance (13b) involves the term

$$Q_{F,ij} = \sum_{m,n} \langle u'_m u'_n u'_i \rangle \mathbf{B}(\mathbf{e}_m, \mathbf{e}_n) \cdot \mathbf{e}_i + \langle u'_m u'_n u'_i \rangle \mathbf{B}(\mathbf{e}_m, \mathbf{e}_n) \cdot \mathbf{e}_j,$$

representing third order interactions  $\langle u'_i u'_j u'_k \rangle$  between modes as well as a linear interaction part represented by  $L_{v,ij} = [\mathbf{L}\mathbf{e}_j + \mathbf{B}(\bar{\mathbf{u}}, \mathbf{e}_j) + \mathbf{B}(\mathbf{e}_j, \bar{\mathbf{u}})] \cdot \mathbf{e}_i$ . The dynamical equations (13a) and (13b) are still not a closed form since we still need to calculate the third order moments  $\langle u'_i u'_j u'_k \rangle$ , which will be further related with higher order moments and become expensive to calculate with the high dimensionality of the system. So the key issue here is to find statistically accurate closure methods to approximate these third order interactions in  $Q_F$ .

The general idea of calculating  $Q_F$  is to run one ensemble of particles for the stochastic coefficients  $u'_j(t; \omega)$  in each direction  $\mathbf{e}_j(t)$  and then to estimate the third order moments by ensemble means. Considering computational efficiency and accuracy, the particle method is only run in a reduced order subspace spanned by  $\{\mathbf{e}_1, \dots, \mathbf{e}_s\}$  with  $s \ll N$ , while the partial basis  $\mathbf{e}_j(t)$  adaptively evolves in time to capture the most important directions of the system according to the *Dynamical Orthogonality* (DO) criterion [30]. The coefficient equations are obtained by a direct Galerkin projection to the DO modes

$$\begin{aligned} \frac{du'_j}{dt} &= \sum_m u'_m [\mathbf{L}\mathbf{e}_m + \mathbf{B}(\bar{\mathbf{u}}, \mathbf{e}_m) + \mathbf{B}(\mathbf{e}_m, \bar{\mathbf{u}})] \cdot \mathbf{e}_j \\ &+ \sum_{m,n} (u'_m u'_n - C_{mn}) \mathbf{B}(\mathbf{e}_m, \mathbf{e}_n) \cdot \mathbf{e}_j, \end{aligned} \quad (14)$$

with  $C_{mn} = \langle u'_m u'^*_n \rangle$ . The dynamical modes evolve according to the equation obtained by stochastic projection of the original equations to the DO coefficients

$$\frac{d\mathbf{e}_j}{dt} = \mathbf{M}_j - \sum_m \mathbf{e}_m (\mathbf{M}_j \cdot \mathbf{e}_m), \quad (15)$$

with

$$\mathbf{M}_j = \mathbf{L}\mathbf{e}_j + \mathbf{B}(\bar{\mathbf{u}}, \mathbf{e}_j) + \mathbf{B}(\mathbf{e}_j, \bar{\mathbf{u}}) + \sum_{m,n,k} \mathbf{B}(\mathbf{e}_m, \mathbf{e}_n) \langle u'_m u'_n u'_k \rangle C_{jk}^{-1}.$$

Although effective in some regimes of weak chaos, this DO closure method by neglecting modes outside the resolved subspace may introduce serious errors in the prediction results. See [16,21] for explicit examples demonstrating this for prediction and Section 2.2.1 for filtering. So more careful calibration using steady state statistics are considered to further improve the model prediction skill. These are the ideas in papers [16,20] for blending the DO method and quasi-linear Gaussian closures. In the numerical tests in this paper, we will focus on four different kinds of closure models listed as follows:

- Quasi-Gaussian (QG) closure filter: only Gaussian features will be considered in this closure model with higher order moments simply neglected, that is, set  $Q_F^{\text{QG}} = 0$  in (13b) with  $s = N$ . This is the classical Gaussian closure [31];
- Modified quasi-Gaussian (MQG) closure filter: this closure method also only calculates the Gaussian features at each time instant but corrects the error from higher order moments using steady state statistics, which can be achieved in advance. Specifically, the steady state third order moments are used to calculate climatology  $Q_{F,\infty}$  independent of time in an efficient fashion. Then in the covariance equation (13b), the nonlinear interaction term  $Q_F$  is replaced by  $Q_F^{\text{MQG}} = Q_F^+(R) + Q_F^-(R)$ , with the first part  $Q_F^+$  from the positive definite part of  $Q_{F,\infty}$  as additional noise while the second term  $Q_F^-$  from the semi-negative definite part of  $Q_{F,\infty}$  as additional damping. See detailed formulas for this method in [21];
- Blended QG-DO filter: this method tries to track the most important third order statistics at each time instant using the dynamical basis as described above. Instead of calculating all the third order moments in the entire high dimensional space, we take a subspace with dimensionality  $s \ll N$  small enough so that the third order statistics can be achieved efficiently with accuracy in this subspace. Thus the nonlinear interaction term  $Q_F^{\text{QGDO}} = Q_F^{V_s}$  is approximated by statistics only in the small subspace  $V_s$  with interactions involving modes outside this subspace neglected as in the QG closure method. Another crucial feature of this method is that the subspace basis  $\mathbf{e}_j(t)$  is designed to evolve adaptively in time according to the DO criterion [30]. Explicit dynamics for the dynamical basis  $\mathbf{e}_j$  as well as the corresponding coefficient  $u'_i$  can be calculated according to this DO criterion as in (14) and (15). This DO criterion helps the resolved subspace to keep tracking the most important directions (that is, directions with largest variances) of the system. Exchange of statistical information between the evolving subspace with non-Gaussian statistics and the evolving Gaussian statistical background is also allowed in this method. See detailed formulas and explanation for this method in [16];
- Blended MQG-DO filter: this method also uses the higher order moments calculated in the adaptive reduced order subspace  $V_s$  as in the QG-DO method, but in addition to that, the unresolved higher order statistics in the orthogonal subspace is further corrected using the steady state information as in the MQG closure. Therefore, the nonlinear interaction term  $Q_F$  in this method is a more detailed calibration about the higher order statistics considering both exact third order statistics in the reduced subspace  $Q_F^{\text{QGDO}}$  at each time instant as well as the correction from steady state information  $Q_F^{\text{MQG}}$  for the unresolved part. The final term becomes  $Q_F^{\text{MQGDO}} = Q_F^{\text{QGDO}} + Q_F^{\text{MQG}} - Q_{F,\infty}^{V_s}$ , with the overlapped part  $Q_{F,\infty}^{V_s}$  subtracted. See detailed formulas and explanation for this method in [20].

Above we just simply introduced the basic ideas about these forecast models. The blended models (QG-DO and MQG-DO) naturally decompose the system into two subspaces with required representations consistent with the mathematical framework described

in Section 2.1.1. Note that the first two forecast models (QG and MQG) only give quasi-Gaussian predictions for the mean and covariance matrix, thus no particle representation is needed and only the Kalman filter update for the mean and covariance is carried out in the analysis step. These can be viewed as special cases of the QG-DO filter or MQG-DO filter with the dimensionality of the particle filter subspace  $\mathbf{u}_1$  set to be zero ( $s = 0$ ). But as we will see in the numerical experiments in Section 4, the MQG Gaussian closure methods can also achieve desirable filtering performance in some dynamical regimes and are more computationally efficient than the blended particle methods although they have less capability in capturing non-Gaussian features. While at the same time, QG closure method is less feasible because too much information about higher order moments is neglected which is crucial for the success of both model prediction and filtering of non-Gaussian features.

**Remark.** The dimensionality of the DO subspace  $s$  has been discussed in [20] for uncertainty quantification schemes. The estimation of the subspace dimensionality  $s$  can be made a priori using steady-state statistics of the dynamical system. It needs to be emphasized here that for the filtering methods  $s$  does not need to be as large as the dimensionality of the attractor (or the number of unstable directions) thanks to the Kalman filter updates in the orthogonal subspace. In the numerical tests in the following sections, we empirically choose  $s = 5$ , which is much smaller than the number of positive Lyapunov coefficients of the system.

## 2.2. Importance of the orthogonal subspace statistics and the adaptively evolving basis

In the algorithms described above, two essential strategies must be noted to guarantee the effectiveness of these methods. First, besides the full statistics in the low dimensional subspace  $\mathbf{u}_1$ , the statistics in the high dimensional orthogonal subspace  $\mathbf{u}_2$  are also taken into account with a conditional Gaussian mixture representation. Second, for the low dimensional subspace  $\mathbf{u}_1$ , rather than using fixed-in-time basis, the subspace is made to evolve in time in order to keep tracking the most energetic directions of the phase space inside the system. It should be emphasized that both strategies are indispensable parts of the algorithms for successfully filtering turbulent dynamical systems. By ignoring the high dimensional orthogonal subspace, even with the first several most important EOF modes (that is, eigenfunctions with the largest eigenvalues for the evolving covariance matrix of the state variables) accurately captured inside a low dimensional subspace, it is still not sufficient to get accurate predictions about the state variables of the system due to the large amount of energy contained inside this orthogonal subspace or the strong nonlinear energy transfers between the resolved most energetic modes and unresolved less energetic ones. On the other hand for the reduced order subspace, a particle method is applied to try to capture the important higher order statistics. With fixed-in-time basis, the most important statistics will be missed at times as the statistics of the system evolve in time. Next we will show the importance of these two issues using simple examples.

The first test model is an extremely simple  $2 \times 2$  linear system with non-normal dynamics [32,16]. Consider a two dimensional variables  $\mathbf{x} = (x, y)^T$  with the dynamics of  $x$  being a deterministic process while stochasticity is introduced in the variable  $y$  so that

$$d\mathbf{x} = \mathbf{A}\mathbf{x}dt + \Sigma d\mathbf{W}_t = \begin{bmatrix} -a & \epsilon_1 \\ \epsilon_2 & -b \end{bmatrix} \mathbf{x}dt + \begin{bmatrix} 0 & 0 \\ 0 & \sigma \end{bmatrix} d\mathbf{W}_t, \quad (16)$$

with  $d\mathbf{W}_t$  white noise. We test the performance of this system in the non-normal regime where the two eigenvectors of the linear coefficient matrix  $\mathbf{A}$  above in (16) cannot be orthogonal to each

other by setting the parameters as  $\epsilon_1 \gg 1, \epsilon_2 = 0$ . As we will see in the examples below, despite the simplicity of this model, it is already sufficient to show the importance of the statistics in the orthogonal subspace. In Appendix A, all the exact solutions for this system and the corresponding equations for dynamical basis and stochastic coefficients are calculated explicitly.

Then a more complex Lorenz-96 (L-96) system [33,34] is used as the major test model for these methods. The L-96 system is a 40-dimensional dynamical system with  $\mathbf{u} = (u_0, u_1, \dots, u_{J-1})^T$

$$\frac{du_j}{dt} = (u_{j+1} - u_{j-2})u_{j-1} - d(t)u_j + F(t), \quad j = 0, 1, \dots, J-1, J = 40. \quad (17)$$

By changing the amplitude of the external forcing  $F$ , the system shows a wide range of different dynamical regimes ranging from weakly chaotic, strongly chaotic, to finally full turbulence with various statistics, which makes it a desirable test model [26]. The dynamics and statistics of the L-96 system in the different regimes with  $F = 5, 6, 8$  utilized here are listed in Appendix B.

To measure the filtering ability of different methods, we use the root mean square error (RMSE) and cross-correlation (XC, or pattern correlation) between the filtered posterior mean from the model and the truth. The formulas for RMSE and XC between two variables  $x$  and  $y$  can be defined by

$$\text{RMSE}(x, y) = \sqrt{\frac{1}{N} \sum_{j=1}^N (x_j - y_j)^2}, \quad (18)$$

$$\text{XC}(x, y) = \frac{\sum_{j=1}^N (x_j - \bar{x})(y_j - \bar{y})}{\sqrt{\sum_{k=1}^N (x_k - \bar{x})^2 \sum_{l=1}^N (y_l - \bar{y})^2}}, \quad (19)$$

with  $\bar{x} = \frac{1}{N} \sum_{j=1}^N x_j$  defined as the mean of the variable. The RMSEs and XCs can be compared either trajectory-wise at each time instant or averaged over time in a statistical steady state to assess the overall performance.

### 2.2.1. Limitation in filtering skill due to ignorance of statistics in the orthogonal subspace

Here we show the necessity of considering the statistics in the orthogonal subspace as described in the algorithm above. Results with the blended particle methods are compared with the particle method constrained inside one subspace as shown below. First, the linear  $2 \times 2$  system in (16) is tested in a strongly non-normal regime with parameters  $a = 4, b = 5, \epsilon_1 = 10, \epsilon_2 = 0, \sigma = 0.5$ . The observation is chosen as a mixture of the modes  $v = G\mathbf{x} + \sigma_0 = x + \alpha y + \sigma_0$  with observation matrix  $G = (1, \alpha)$ . Considering the steady state variance and decorrelation time  $\text{var}(\mathbf{x}) = (0.0694, 0.0250)$  and  $T_{\text{corr}}(\mathbf{x}) = (0.45, 0.20)$ , we choose the observation time step  $\Delta t = 0.05$ , shorter than the decorrelation time for both modes  $x$  and  $y$ . Two sets of observation noises  $\sigma_0^2 = 0.01, 0.03$  are tested. The first one is smaller than the averaged energy and the second one is slightly larger than the average. Three different filtering methods are compared:

- QG-DO blended filter in one-dimensional subspace: run fully resolved dynamics in the one-dimensional DO subspace as in (A.5) and (A.6) (see Appendix A) in the forecast step, and in the analysis step use the blended filtering method (that is, run particle filter in  $\mathbf{e}_1$  direction, and Kalman filter with conditional Gaussian assumption in the orthogonal direction). The exact solution of the mean and covariance matrix (A.3), (A.4) (Appendix A) is used;

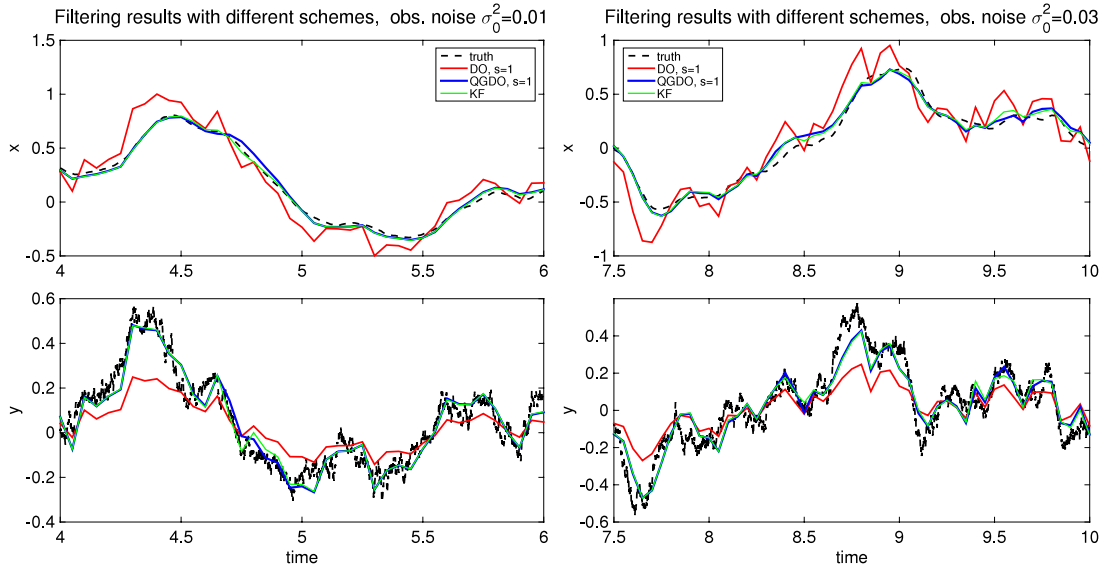


**Fig. 1.** Filtering results for time series of the two components  $x$  and  $y$  from the  $2 \times 2$  linear system using blended QG-DO method (blue), particle method in 1-d dynamical subspace (red), compared with the optimal Kalman filter (green). The true solutions are shown by black dashed lines. One dimensional mixed noised observation  $v = x + y + \sigma_0$  is used in the model with two different noise amplitudes  $\sigma_0^2 = 0.01$  and  $\sigma_0^2 = 0.03$ . (For interpretation of the references to color in this figure legend, the reader is referred to the web version of this article.)

**Table 1**

RMS errors and cross correlations (in parentheses) for variable  $x$  and  $y$  from the  $2 \times 2$  linear system with different methods. The observation is  $v = x + y + \sigma_0$ . Results for two different noise amplitudes  $\sigma_0^2 = 0.01$  and  $\sigma_0^2 = 0.03$  are listed.

Mode	Method		
	DO	QG-DO	Kalman filter
(a) Observation error $\sigma_0^2 = 0.01$			
$x$	0.1132 (0.9621)	0.0382 (0.9922)	0.0369 (0.9927)
$y$	0.1009 (0.9166)	0.0640 (0.9340)	0.0634 (0.9353)
(b) Observation error $\sigma_0^2 = 0.03$			
$x$	0.1384 (0.9311)	0.0573 (0.9801)	0.0537 (0.9825)
$y$	0.1092 (0.8700)	0.0857 (0.8774)	0.0845 (0.8814)

- DO filtering in dynamical one-dimensional subspace: get the exact mean and covariance by (A.3), (A.4), but only run one-dimensional subspace dynamics in the forecast model to calculate  $(\mathbf{e}_1, u_1)$ , and filter the prior  $\mathbf{x} = \bar{\mathbf{x}} + u_1 \mathbf{e}_1$  with the observation data using standard particle filter. After each analysis step, recalculate the principal direction  $\mathbf{e}_1$  using the exact solution of  $R$ , and resample to get the particle presentation of  $u_1$ ;
- Standard Kalman filter: because the system and observation are both linear and Gaussian, the optimal filtering result can be achieved by Kalman filter. Therefore we also check Kalman filter here for comparison.

Note that in the methods above, the first one is exactly the blended particle method described in Section 2 with QG-DO model in the forecast step applied to the linear system. Considering that only linear dynamics occurs in the system with only Gaussian statistics concerned, it is enough only to use the simpler QG method rather than MQG. The second method is like a pure particle filter inside a subspace. It only tries to resolve and filter the most important direction and ignores the other one. Here with the help of the exact solution, the principal direction can be calculated exactly. The particles can always keep tracking the most energetic direction with accuracy, so the only source of error comes from the ignorance of the second direction containing little energy.

In Fig. 1 the filtering results for time series of the two components  $x$  and  $y$  with all the three methods described above are compared with the truth from the exact solution. The observation

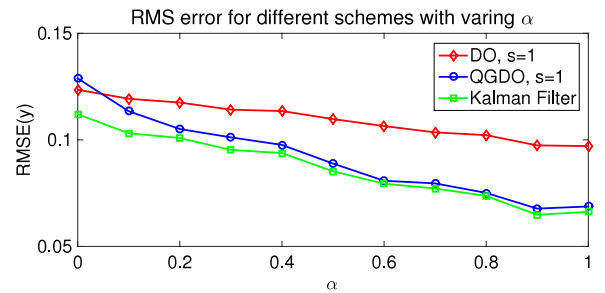


**Fig. 2.** Comparison of RMSEs for component  $y$  from the  $2 \times 2$  linear system with different observations  $v = x + \alpha y + \sigma_0$ ,  $\alpha \in [0, 1]$ ,  $\sigma_0^2 = 0.01$ ,  $\Delta t = 0.05$ . Results with blended QG-DO method (blue), particle method in 1-d dynamical subspace (red), and Kalman filter (green) are compared. (For interpretation of the references to color in this figure legend, the reader is referred to the web version of this article.)

data is a balanced mixture of the two components as  $v = x + y + \sigma_0$  with two different observation noise amplitudes  $\sigma_0^2 = 0.01$  and  $\sigma_0^2 = 0.03$ . The results for the blended QG-DO methods almost overlap the optimal Kalman filter results in this linear model with both noise amplitudes, and they are both close to the truth from the exact solutions in dashed black lines. However, for the DO particle filter with one most energetic direction of the 2 dimensional model accurately captured by particles, large filtering errors still appear in both cases and both components  $x$  and  $y$ . For comparisons in more detail the corresponding numbers for the RMSEs and pattern correlations as defined in (18) and (19) are listed in Table 1. It can be seen that blended QG-DO method gives similar small errors and pattern correlations with the Kalman filter results while DO particle filter results in much larger errors and smaller pattern correlations. Fig. 2 shows RMSEs of the stochastic component  $y$  with different kinds of observations  $v = x + \alpha y + \sigma_0$ ,  $\alpha \in [0, 1]$ . For weakly observed case  $\alpha \ll 1$  or even unobservable case  $\alpha = 0$ , little information can be got from the observations for  $y$  so particle values are poorly guided to capture the randomness in  $y$ . Thus both QG-DO and DO methods share relatively similar error (whereas Kalman filter is better since it uses the exact solution of  $y$  component in the forecast model so it can achieve an estimate with error amplitude comparable to the observation noise  $\sigma_0$ ). As the observability of  $y$  increases, blended

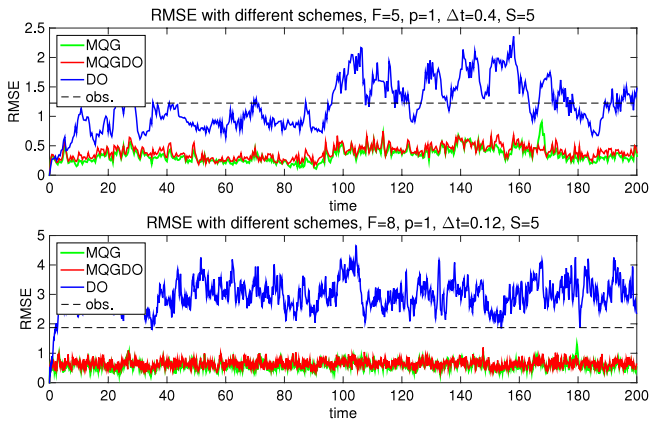


**Fig. 3.** RMSEs with different filtering methods for filtering L-96 system in weakly chaotic regime ( $F = 5$ , upper) and strongly chaotic regime ( $F = 8$ , lower) with plentiful observations at every grid point. Results for only filtering the subspace represented by the first five most energetic dynamical basis modes using particle filter (blue) are compared with MQG filter (green) and blended MQG-DO filter (red). The dashed black line marks the amplitude of the observation noise. (For interpretation of the references to color in this figure legend, the reader is referred to the web version of this article.)

method QG-DO becomes superior to DO method increasingly, and has similar errors with Kalman filter results. To summarize, with even only a one-dimensional orthogonal subspace neglected and tracking the most energetic direction of the system calculated by the covariance  $R$  from exact solution, it is still insufficient for the pure particle filtering method to capture the true dynamics with accuracy in the non-normal regime. The filtering performance can be greatly improved by incorporating the statistics in the orthogonal subspace by taking the QG-DO filter. The filtering results become comparable with the optimal Kalman filter.

In the second model, we test the same issue further with the more complicated 40-mode L-96 system. Since the system has nonlinearities and non-Gaussian statistics, we choose the blended MQG-DO filter and MQG closure filter here with higher order moments corrections included, compared with the DO particle only in the reduced order subspace with no statistics considered in the orthogonal part. The dimensionality of the reduced subspace for particle filter is chosen as  $s = 5$  and dynamical basis is adaptive and tries to get the principal most energetic modes. Two dynamical regimes of weakly chaotic  $F = 5$  and turbulent  $F = 8$  dynamics are tested, and full observations of every grid point are used. In Fig. 3 we run a particle filter for the reduced order dynamical subspace captured by the first five most energetic modes and ignore the orthogonal subspace. The results are compared with the MQG filter and blended MQG-DO filter (see Section 4 for more detailed discussion and results for these filtering methods). The RMSEs for DO particle methods become quite large even in this case with plentiful observations and are above the observation error without filtering while blended MQG-DO method and MQG method give similar small errors. This is an especially powerful demonstration for  $F = 5$  with plentiful observation since there are two dominant energetic modes,  $s = 5$ , and we have plentiful observations. Thus, it can be seen that only by adding Gaussian statistics in the large orthogonal subspace (as in MQG) can large improvements for filtering performance be achieved.

### 2.2.2. Limitation in filtering skill due to fixed-in-time basis

Here we go on to test another aspect of the algorithms using a dynamical basis. In the low dimensional subspace with full statistics resolved by particles, one possible guess is that using the fixed basis from the principal eigendirections of the covariance matrix in steady state might give comparable results as filtering with the dynamically evolving subspace, especially for  $F = 5$ .

We will test this using again the 40-mode L-96 model. The fixed basis method is tested by taking also the first five most energetic Fourier modes but from the statistical stationary state. The filter is applied in the same way as the blended particle filter in two subspaces only with this fixed-in-time subspace basis. Thus in this method, there is no need to update the dynamical basis as in the algorithms described above and the other strategies in both two subspaces will be carried out with particle representations in one subspace and conditional Gaussian corrections in the other subspace correspondingly. Again we compare this method with the blended MQG-DO filter with evolving basis and MQG closure filter in two dynamical regimes  $F = 5$  and  $F = 8$  with full observations at each grid points. In Fig. 4, the RMSEs for the fixed basis filter are compared with the blended filter results. It can be seen that the fixed-in-time filter suffers frequent filter divergence while the blended filter with dynamical subspace basis keeps performing well. The reason for this serious filter divergence can be shown by checking the fraction of total energy contained in the fixed subspace. As in the second row of Fig. 4, the portion of energy in the fixed subspace changes as the system evolves with time. The statistics of the system evolve in time and will not always be confined inside the same steady state subspace. At some particular time instants the energy in the fixed subspace reaches extremely small values, making nearly no energy left in the subspace. As a consequence, the particles in the subspace with little energy (variance) will collapse altogether and diverge at these time instants ending up with large filtering errors. Therefore although we can choose fixed basis representing the most important directions in steady state, the statistics for the system still change directions as they evolve in time. Ignoring this time dependent dynamical feature of the principal directions will lead to serious particle divergence with failure in capturing the right amount of higher order statistics in the key subspace of interest. For the MQG closure filter, it adopts fixed basis but includes no particle representations. So particle collapse is not a problem for this method; thus in this test regime, the MQG filter gives comparable results with the blended MQG-DO filter (Section 4 will show the deficiencies of the MQG method compared with the MQG-DO filter in strong non-Gaussian regime).

### 3. Practical strategies for realizability and stability

In the previous section we introduce the basic mathematical framework of the blended filtering algorithms and illustrate several important aspects of the methods by examples. Still to achieve desirable performance of the blended filtering methods, several practical numerical treatments should be considered to make sure that the schemes are both accurate and efficient in computing. These issues follow from the realizability and stability features of the methods. That is, we need to make sure that the estimated state variables in particle forms are consistent in statistics with the predicted mean and covariance and the positive definite property of the estimated conditional covariance matrix must be preserved, otherwise filter divergence and instability of the schemes will take place. The first problem comes from finding the most probable conditional distribution  $p(\mathbf{u}_2|\mathbf{u}_1)$  in the orthogonal subspace  $\mathbf{u}_2$  given the particle representation in the  $\mathbf{u}_1$  subspace as needed in (3). Below, through information theory a conditional Gaussian distribution  $\mathcal{N}(\bar{\mathbf{u}}_2(\mathbf{u}_1), R_2^-)$  is achieved and a realizable condition for  $R_2^-$  (that is,  $R_2^-$  to be positive-definite) is established. The second problem concerns the stability of the particle samples, which is also tightly related with the realizability condition. Proper inflation should be added to the particles in the resample process to avoid particle collapse. These practical strategies which are key to the accuracy of the filtering methods are discussed and illustrated by some examples in this section.

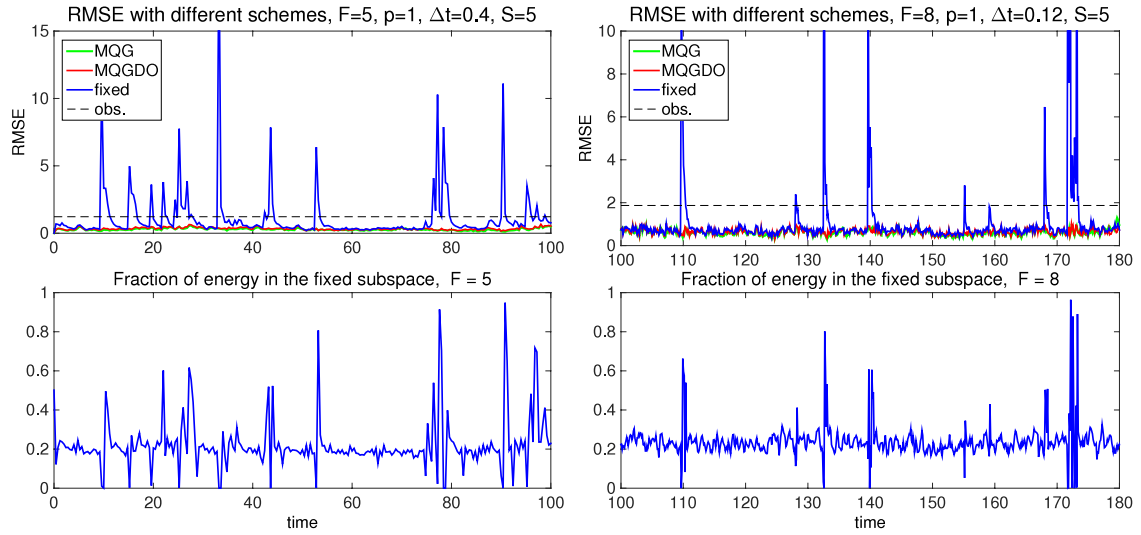


**Fig. 4.** Limitations by using fixed-in-time basis: the first row shows the RMSEs from filtering results with fixed subspace basis defined by first 5 leading principal EOFs (blue) compared with the MQG filter (green) and the blended MQG-DO filter with dynamical basis (red). Two different regimes  $F = 5$  and  $F = 8$  are tested with plentiful observations at every grid point, and the dashed black line shows the amplitude of observation error. In the second row, the corresponding energy contained in the fixed-in-time subspace basis are compared with the filtering errors above. (For interpretation of the references to color in this figure legend, the reader is referred to the web version of this article.)

### 3.1. The most probable conditional distribution $p(\mathbf{u}_2|\mathbf{u}_1)$ through information theory

As described in (7), in part I of the blended algorithm, the forecast statistics supplied at each analysis time are the following:

(A) A particle approximation for the marginal distribution

$$p_-(\mathbf{u}_1) = \sum_{j=1}^Q p_{j,-} \delta(\mathbf{u}_1 - \mathbf{u}_{1,j});$$

(B) The mean  $\bar{\mathbf{u}}_2^-$  and the covariance matrix

$$R = \begin{pmatrix} R_1 & R_{12} \\ R_{12}^T & R_2 \end{pmatrix}.$$

The goal here is to find an efficient way to use these statistics to build the forecast prior distribution with the form in (3) with a conditional Gaussian distribution.

The maximum-entropy principle from information theory tells that the least biased most probable distribution should maximize the entropy defined as  $\mathcal{H}[p] = -\int_{\mathbb{R}^N} p(\mathbf{u}) \log p(\mathbf{u}) d\mathbf{u}$  [27]. With the help of this principle, the problem can be rephrased as to find the distribution  $p^* = p^*(\mathbf{u}_2|\mathbf{u}_1)$ , such that,

$$p^*(\mathbf{u}_2|\mathbf{u}_1) = \operatorname{argmax}_{p \in \mathcal{C}} \int p_-(\mathbf{u}_1) \mathcal{H}[p(\mathbf{u}_2|\mathbf{u}_1)] d\mathbf{u}_1, \quad (20)$$

under the constraints  $\mathcal{C}$  of consistent statistics for the mean  $\bar{\mathbf{u}}_2$  and covariance  $R_2$  in the  $\mathbf{u}_2$  subspace as well as the cross-covariance  $R_{12}$  between the two subspaces from the prior distribution. This most probable conditional distribution  $p(\mathbf{u}_2|\mathbf{u}_1)$  can be found formally via the method of variations. Taking variations of the entropy and constraints  $\mathcal{C}$ , the method of Lagrangian multipliers shows that indeed a Gaussian distribution gives the optimal distribution that maximizes the entropy in (20). A detailed derivation of this result is stated in Appendix C. Furthermore, through the derivation of the max-entropy solution, it can be shown that for the conditional Gaussian distribution  $\mathcal{N}(\bar{\mathbf{u}}_{2,j}^-, R_2^-)$  conditional on values  $\mathbf{u}_{1,j}$  in the low dimensional subspace, only the conditional mean  $\bar{\mathbf{u}}_{2,j}^-$  is dependent on different particle values while the conditional

covariance  $R_2^-$  can be expressed universally as

$$\begin{aligned} R_2^- &= R_2 - \int \bar{\mathbf{u}}_2'(\mathbf{u}_1) \otimes \bar{\mathbf{u}}_2'(\mathbf{u}_1) p(\mathbf{u}_1) d\mathbf{u}_1 \\ &= R_2 - \sum_j \bar{\mathbf{u}}_{2,j}' \otimes \bar{\mathbf{u}}_{2,j}' p_j. \end{aligned} \quad (21)$$

Therefore with the help of information theory, the prior covariance  $R_2$  from the forecast model is decomposed into two separate parts. The first part is represented by the fluctuation of each conditional mean  $\bar{\mathbf{u}}_{2,j}' = \bar{\mathbf{u}}_{2,j}^- - \langle \mathbf{u}_2 \rangle$ , and for each particle the uncertainty is further quantified by an additional covariance  $R_2^-$  (independent of  $\mathbf{u}_{1,j}$ ) calculated by (21). The fact that  $R_2^-$  is independent of the choice of particles in  $\mathbf{u}_{1,j}$  is extremely important for reducing the computational cost for the large scale piece of the covariance matrix when high-dimensional problems are applied, and this property will be exploited further in the following steps. However, at this stage a proper way of getting the values of the conditional mean  $\bar{\mathbf{u}}_{2,j}'$  is unclear, whereas the above results infer that it is reasonable to make use of the max-entropy property. Then the issue becomes how to find a computational affordable way to approximate the max-entropy solution which is consistent with the forecast statistics.

#### 3.1.1. Solving the underdetermined system

The conditional mean fluctuations  $\bar{\mathbf{u}}_{2,j}' = \bar{\mathbf{u}}_{2,j}^- - \langle \mathbf{u}_2 \rangle$  can be solved by enforcing the consistent condition for the mean and cross-covariance of the forecast result, i.e.

$$\begin{aligned} \bar{\mathbf{u}}_2^- &= \iint \mathbf{u}_2 p_-(\mathbf{u}_1) p(\mathbf{u}_2|\mathbf{u}_1) d\mathbf{u}_1 d\mathbf{u}_2 \\ &= \int \bar{\mathbf{u}}_2(\mathbf{u}_1) p_-(\mathbf{u}_1) d\mathbf{u}_1, \\ R_{12} &= \iint (\mathbf{u}_1 - \bar{\mathbf{u}}_1^-) \otimes (\mathbf{u}_2 - \bar{\mathbf{u}}_2^-) p_-(\mathbf{u}_1) p(\mathbf{u}_2|\mathbf{u}_1) d\mathbf{u}_1 d\mathbf{u}_2 \\ &= \int (\mathbf{u}_1 - \bar{\mathbf{u}}_1^-) \otimes (\bar{\mathbf{u}}_2(\mathbf{u}_1) - \bar{\mathbf{u}}_2^-) p_-(\mathbf{u}_1) d\mathbf{u}_1. \end{aligned}$$

Here the conditional mean  $\bar{\mathbf{u}}_2(\mathbf{u}_1) = \int \mathbf{u}_2 p(\mathbf{u}_2|\mathbf{u}_1) d\mathbf{u}_2$  is defined through the conditional measure  $p(\mathbf{u}_2|\mathbf{u}_1)$  in the  $\mathbf{u}_2$  subspace.

In terms of the discrete representation, the above system can be written as a linear system

$$\begin{bmatrix} p_1 u_{1,1}^{1'} & \cdots & p_Q u_{1,1}^{Q'} \\ \vdots & \ddots & \vdots \\ p_1 u_{1,N_1}^{1'} & \cdots & p_Q u_{1,N_1}^{Q'} \\ p_1 & \cdots & p_Q \end{bmatrix}_{(N_1+1) \times Q} \times \begin{bmatrix} u_{2,1}^{1'} & \cdots & u_{2,N_2}^{1'} \\ u_{2,1}^{2'} & \cdots & u_{2,N_2}^{2'} \\ \vdots & \ddots & \vdots \\ u_{2,1}^{Q'} & \cdots & u_{2,N_2}^{Q'} \end{bmatrix}_{Q \times N_2} = \begin{bmatrix} R_{12} \\ 0 \end{bmatrix}_{(N_1+1) \times N_2}. \quad (22)$$

For simplicity following we will denote this system abstractly as  $\mathcal{L}U_2 = \mathcal{F}$ . In general cases with sufficient ensemble size  $Q \gg N_1 + 1$ , the linear system above is highly underdetermined with infinite many solutions. Motivated by the max-entropy principle described above, the redundancy can be reduced by seeking among the solutions in (22) the optimal one which maximizes the entropy

$$\mathbf{u}_2^* = \operatorname{argmax}_{\mathbf{u}_2} \mathcal{J}[p_G(\mathbf{u}_2|\mathbf{u}_1)]. \quad (23)$$

Here the target distribution  $p_G(\mathbf{u}_2|\mathbf{u}_1)$  is conditional Gaussian, thus the expression for the entropy can be simplified with simple calculation [27] as

$$\mathcal{J}[p_G(\mathbf{u}_2|\mathbf{u}_1)] = \frac{1}{2} \log \det(R_2^-) + \frac{N_2}{2} (\log 2\pi - 1). \quad (24)$$

Combining the expressions in (21), (23) and (24), we need to find the optimal solution  $\mathbf{u}_2^*$  of the linear system (22) such that the logarithm of the determinant of the conditional covariance is maximized

$$\begin{aligned} \bar{\mathbf{u}}'_{2,j} &= \operatorname{argmax} \log \det \left( R_2 - \sum_j p_j \bar{\mathbf{u}}'_{2,j} \otimes \bar{\mathbf{u}}'_{2,j} \right) \\ &= \operatorname{argmax} \log \det \left( I - \sum_j \left( p_j^{1/2} R_2^{-1/2} \bar{\mathbf{u}}'_{2,j} \right) \right. \\ &\quad \left. \otimes \left( p_j^{1/2} R_2^{-1/2} \bar{\mathbf{u}}'_{2,j} \right) \right). \end{aligned} \quad (25)$$

This nonlinear optimization problem described above involving the determinant of a large scale matrix is way too expensive considering the high dimensionality of  $N_2$  subspace. But note that the fluctuation  $\bar{\mathbf{u}}'_{2,j}$  from the linear system (22) is calculated using the cross-covariance  $R_{12}$ , which is assumed to be small representing the weak correlations between the two subspaces (in fact, in the ideal situation with  $P$  in (7) as the exact eigendirections of  $R$ , the transformed matrix  $R_t$  under the eigenbasis becomes diagonal and  $R_{12}$  becomes exactly 0). Therefore it is a reasonable assumption to assume  $\|R_{12}\| \sim O(\epsilon)$  and  $\|\bar{\mathbf{u}}'_{2,j}\| \sim \|\mathcal{L}^\dagger \mathcal{F}\| \sim O(\epsilon)$  with  $\epsilon \ll 1$  and the linear system (22) denoted abstractly as  $\mathcal{L}U_2 = \mathcal{F}$  with the pseudoinverse operator  $\mathcal{L}^\dagger$  assumed to be bounded. Using the asymptotic expansion of the determinant

$$\det(I - \epsilon A) = -\epsilon \operatorname{tr} A + O(\epsilon^2). \quad (26)$$

One proper estimation for the determinant in (25) is to seek a first-order approximation by minimizing the trace of the matrix  $A$ . Note also that each component of  $\bar{\mathbf{u}}'_{2,j}$  is calculated column-wise independent with each other in the linear system (22), seeking the optimal solution minimizing each mode under the  $L_2$ -norm  $\|p_j^{1/2} R_2^{-1/2} \bar{\mathbf{u}}'_{2,j}\|_2$  is sufficient. Thus, the least-squares solution can be solved easily by taking the pseudo-inverse of the coefficient matrix of the linear system. However, the first-order approximation described above still requires calculating the

inverse square-root of the covariance matrix  $R_2$ , which becomes computational forbidden given the high dimensionality of the problems. A further simplification is to consider minimizing the  $L_2$ -norm  $\|p_j^{1/2} \bar{\mathbf{u}}'_{2,j}\|_2$  instead. In fact, it is not hard to check that

$$\begin{aligned} &\operatorname{tr} \sum_j \left( p_j^{1/2} R_2^{-1/2} \bar{\mathbf{u}}'_{2,j} \right) \otimes \left( p_j^{1/2} R_2^{-1/2} \bar{\mathbf{u}}'_{2,j} \right) \\ &= \sum_j p_j \operatorname{tr} \left( \bar{\mathbf{u}}'_{2,j} \otimes \bar{\mathbf{u}}'_{2,j} R_2^{-1/2} R_2^{-1/2} \right) \\ &= \operatorname{tr} \left[ \left( \sum_j p_j^{1/2} \bar{\mathbf{u}}'_{2,j} \otimes p_j^{1/2} \bar{\mathbf{u}}'_{2,j} \right) \cdot R_2^{-1} \right]. \end{aligned}$$

Use the trace inequality  $\lambda_1(A) \operatorname{tr} B \leq \operatorname{tr} AB \leq \lambda_n(A) \operatorname{tr} B$ , for positive semidefinite matrices  $A, B$  with  $\lambda_1, \lambda_n$  the smallest and largest eigenvalues, and that  $R_2^-$  is independent of  $j$  here (result from the max-entropy solution). Therefore, the approximation using least-squares solution of  $p_j^{1/2} \bar{\mathbf{u}}'_{2,j}$  instead of  $p_j^{1/2} R_2^{-1/2} \bar{\mathbf{u}}'_{2,j}$  is always appropriate given that the condition number of  $R_2^{-1}$  is not too large, i.e.  $\kappa(R_2^{-1}) \sim 1$ , which is actually a prerequisite for the decomposed subspace  $\mathbf{u}_2$  (and actually, a case with too large a condition number,  $\kappa(R_2^{-1}) \gg 1$ , is often a sign of serious filter divergence).

For practical implementations, the two approaches can both be carried out with simple rearrangements of the linear system (22):

(A) Minimizing the  $L_2$ -norm  $\|p_j^{1/2} R_2^{-1/2} \bar{\mathbf{u}}'_{2,j}\|_2$ : solve the least-squares solution of  $\tilde{\mathcal{L}}V_2 = \tilde{\mathcal{F}}$  by defining

$$\tilde{\mathcal{L}} = \mathcal{L}W^{-\frac{1}{2}}, \quad \tilde{\mathcal{F}} = \mathcal{F}R_2^{-\frac{1}{2}}, \quad V_2 = W^{\frac{1}{2}}U_2R_2^{-\frac{1}{2}},$$

with  $W = \operatorname{diag}_j \{p_j\}$ .

(B) Minimizing the  $L_2$ -norm  $\|p_j^{1/2} \bar{\mathbf{u}}'_{2,j}\|_2$ : solve the least-squares solution of  $\tilde{\mathcal{L}}V_2 = \tilde{\mathcal{F}}$  by defining

$$\tilde{\mathcal{L}} = \mathcal{L}W^{-\frac{1}{2}}, \quad \tilde{\mathcal{F}} = \mathcal{F}, \quad V_2 = W^{\frac{1}{2}}U_2,$$

with  $W = \operatorname{diag}_j \{p_j\}$ .

The least-squares problem above can be easily solved by applying Moore–Penrose pseudoinverse of  $\tilde{\mathcal{L}}$ . The two different approaches with slight difference can be chosen according to the scale and complexity of the problem, whereas the second one is always preferred since it is much cheaper and exhibits no obvious deficiency in practical implementations. We will always use the second approach in the numerical tests in the next section.

### 3.1.2. Corrections for realizability

Finally note that the above solutions of  $\bar{\mathbf{u}}'_2$  from the least squares solution for both the two approaches may not guarantee the positive-definite requirement for the covariance  $R_2^-$  in (21), that is, realizability may still be violated. With unrealizable covariance  $R_2^-$ , the condition number  $\kappa(R_2^{-1})$  may explode, resulting a meaningless approximation for the fluctuation terms  $\bar{\mathbf{u}}'_2$ . In theory,  $R_2^-$  is defined as the covariance matrix for  $\bar{\mathbf{u}}_2^-(\mathbf{u}_1) - \bar{\mathbf{u}}_2^-$  under the optimal measure  $p^*(\mathbf{u}_2|\mathbf{u}_1)$ , showing that the conditional covariance  $R_2^-$  will always stay positive-definite given that the maximum-entropy solution of  $\bar{\mathbf{u}}_2(\mathbf{u}_1)$  is chosen. However the maximum-entropy problem may not have a solution and as described above, the least squares solutions are at most a first order approximation for the max-entropy solution. Therefore realizability in our approach is not certainly guaranteed and needs to be checked. On the other hand, to check each of the eigenvalues of the covariance matrix requires eigenvalue decomposition of the

large scale matrix  $R_2^- = R_2 - \sum_j \bar{\mathbf{u}}'_{2,j} \otimes \bar{\mathbf{u}}'_{2,j} p_j$ . To reduce this computational cost, note that the correction term here is the sum of a series of rank 1 matrix  $\bar{\mathbf{u}}'_{2,j} \otimes \bar{\mathbf{u}}'_{2,j} p_j$  with eigenvector  $\bar{\mathbf{u}}'_{2,j}$ . Then realizability checking can be achieved by adding an extra inflation term  $\alpha_j \in [0, 1]$  according to each direction  $\bar{\mathbf{u}}'_{2,j}$  such that

$$R_2^- = R_2 - \sum_j \alpha_j p_j \bar{\mathbf{u}}'_{2,j} \otimes \bar{\mathbf{u}}'_{2,j}.$$

Here the inflation coefficients  $\alpha_j$  can be chosen according to

- $\alpha_j = 1$ , if  $\bar{\mathbf{u}}_{2,j}^T (R_2 - \sum_k \bar{\mathbf{u}}'_{2,k} \otimes \bar{\mathbf{u}}'_{2,k} p_k) \bar{\mathbf{u}}'_{2,j} > \epsilon_0$ ;
- $\alpha_j = 1 - \frac{\epsilon_0 - \bar{\mathbf{u}}_{2,j}^T (R_2 - \sum_k \bar{\mathbf{u}}'_{2,k} \otimes \bar{\mathbf{u}}'_{2,k} p_k) \bar{\mathbf{u}}'_{2,j}}{p_j |\bar{\mathbf{u}}'_{2,j}|^4}$ , otherwise;

where  $\epsilon_0 \ll 1$  is a small number chosen to avoid numerical errors, and  $1 \leq j \leq Q$ . Then this process should be done for all the  $Q$  ensemble members, making this process not a quite efficient one. In an even simpler algorithm, we inflate the conditional covariance to its upper bound, that is, set

$$R_2^- = R_2 \geq 0.$$

This is the crudest correction and positive definite property will always be satisfied in this case. As we will see in the examples following, for QG-DO filter with smaller variances in the orthogonal subspace, this maximum inflation can effectively improve the filter performance. For MQG-DO filter, the realizability condition is seldom violated due to the accurate prediction from the more sophisticated prediction model and we use the above algorithm as needed.

### 3.2. Stability of the schemes and resampling strategies

In applications of particle methods, another issue that needs to be addressed is about particle collapse. The normalized particle weights  $p_j$  tend to concentrate on a few values (or with even one particle with importance weight near 1) as time evolves. The over-concentration of particles could even be typical in low dimensional problems. Furthermore, for the blended schemes, particle collapse is also related with the violation of the realizability condition of the covariance  $R_2^-$ . Through (21), it can be found that the matrix  $R_2^-$  becomes non-positive definite when the fluctuation variance  $\sum_j \bar{\mathbf{u}}'_{2,j} \otimes \bar{\mathbf{u}}'_{2,j} p_j$  becomes larger compared with the forecast result  $R_2$ . This is tightly related to the collapse of the particles. In fact, the covariance matrix  $R$  approximated by the particles will become extremely small when particles degenerate to only a few values; and in turn the unrealizable covariance  $R_2$  will further intensify particle collapse. Therefore to inherently remove the danger of unrealizable issues, we should consider the stability of the particle method.

The common strategy to stabilize the scheme is to perform resampling sufficiently often [24]. The idea in resampling is to duplicate particles with larger weights and remove the other ones with negligible weights. This process can be viewed as adding extra variances or noises into the particle system and inflating the corresponding covariance. Specifically, in stochastic systems, the extra variance can be added automatically through the internal uncertainty by integrating the model in further steps; for deterministic systems like the L-96 model, additional noises with small amplitude needed to be added artificially to each duplicated particle to enhance the diversity of particle values. One popular resampling strategy is the residual resampling [24] which is an efficient way to decrease the variance added due to the process.

Especially here, we consider the additional noise added to each duplicated particles for deterministic systems. It can be noticed that particle collapse is strongly related with the prediction skill of the forecast model. Less accurate predictions require larger variance added to the particle values as a compensation, whereas

the amplitude of the noises needs to be controlled to avoid unrealizability such that  $R_2^- = R_2 - \sum_j p_j \bar{\mathbf{u}}'_{2,j} \otimes \bar{\mathbf{u}}'_{2,j} \geq 0$ , where too large noises may overinflate the second term on the right side (for example, by applying the QG-DO model, the forecast covariance  $R_2$  is easy to become extremely small since the high order nonlinear interaction is cut off between the two subspaces, thus making the violation of realizability quite easy to take place). One may hope that smaller noises are added when the predictions from most ensemble members are relatively good, while larger variances should be introduced to the particles to give better corrections if the errors become larger. Here we propose one possible way to add the inflation of the variance adaptively in the resampling process. The effective ensemble size  $N_{\text{eff}}$  introduced in [24]

$$N_{\text{eff}} = \frac{1}{\sum_{j=1}^Q p_j^2},$$

can be used as one measure for the amount of particles which have relatively good approximations about the state variables. Note that  $1 \leq N_{\text{eff}} \leq Q$ . Larger noises as a correction term should be added during resampling when serious particle collapse takes place, say  $N_{\text{eff}} \sim 1$ ; and on the other hand the inflation needs to be kept small when most of the particles have desirable values, say  $N_{\text{eff}} \sim Q$ , thus no extra noises will be introduced to the system. According to this, the inflation added to each resampled particle is given as a white noise with the variance measured as

$$\sigma^2 = (M - m) \exp\left(\frac{1 - N_{\text{eff}}}{2}\right) + m, \quad (27)$$

where  $M$  and  $m$  control the largest and smallest inflations added. The values can be chosen according to the prior variances of the particles. The noises increase exponentially when particles collapse. With this exponential function, large additional noise will be added only when the effective ensemble size  $N_{\text{eff}}$  becomes extremely small, that is, close to collapse. Thus in general cases no strong perturbations will be introduced to destroy the statistics captured from the forecast model.

In general, the resampling process can be summarized as follows:

**Algorithm. (Resampling)** If the effective particle number becomes less than some threshold,  $N_{\text{eff}} < M$  ( $M = Q/2$ , say), begin this resampling process.

- Duplicate or remove particles according to their weights  $p_j$  using some standard strategy (residual resampling, say);
- For the duplicated particles  $\mathbf{u}_j$  with  $k_j$  copies, add a small Gaussian perturbation  $\mathbf{v} \sim \mathcal{N}(\mathbf{0}, \sigma^2)$  to each particle,
 
$$\bar{\mathbf{u}}_j = \mathbf{u}_j + \mathbf{v},$$
 with  $\sigma^2$  calculated as in (27);
- Assign the particle weights to be uniform  $p_j = \frac{1}{Q}$ .

### 3.3. Realizability and stability check using L-96 system

Here again, we check the realizability and stability issues using the L-96 system (17). First, as already mentioned before, maximum inflated conditional covariance matrix  $R_2^- = R_2$  rather than the statistical consistent form (21) should be applied for QG-DO filter, which underestimates the energy inside the orthogonal subspace  $\mathbf{u}_2$  due to its cut-off of third order interaction. Fig. 5 shows the RMS errors for QG-DO filter with both inflated  $R_2^-$  and its original form compared with the MQG-DO result. Here we use  $F = 5$  with complete observations. It can be seen that QG-DO filter becomes easier to diverge with no inflation added to  $R_2$ . The reason can be explained from the plots for the fraction of energy in the  $\mathbf{u}_2$

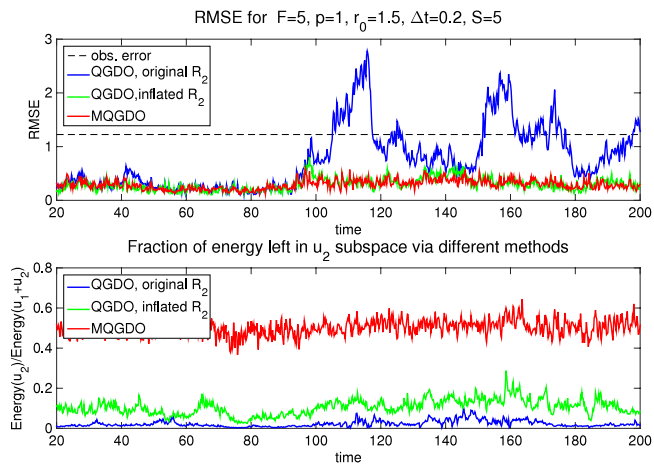


**Fig. 5.** The necessity of using inflated  $R_2$  covariance matrix in QG-DO model. First row: The RMSEs for QG-DO schemes with and without  $R_2$  inflation compared with the MQG-DO results in regime with plentiful observations  $p = 1$  and moderate observation time  $\Delta t = 0.2$  for  $F = 5$ . Second row: the fraction of energy in the  $u_2$  subspace corresponding to the three methods on the left.

subspace, shown in the right panel. MQG-DO method can achieve a large amount of energy in the orthogonal subspace due to its more careful calibration about the statistics in this subspace, whereas the original QG-DO method captures very little energy in this subspace. With a little inflation from  $R_2$  for QG-DO filter, the total variance in  $u_2$  subspace can get increased, thus effectively avoiding serious filter divergence as in the original case.

Second, we can check the stability of these filtering strategies. Here we test the model in a typical regime with extremely small observation noise  $r_0 = 0.01$  and long observation time  $\Delta t = 0.25$  close to the decorrelation time for strongly chaotic dynamics  $F = 8$ . Also regularly spaced sparse observations  $p = 4$  are used. This regime of high quality sparse space-time observations is a difficult test for particle methods [26, chap. 15]. The first two rows of Fig. 6 show the time series of RMS errors and pattern correlations running for a long time  $T = 1000$  using MQG filter, MQG-DO filter, and QG-DO filter with the adaptive resample strategy as described above. Only MQG filter diverges for a short time and converges again quickly during this long process. The third row of Fig. 6 plots the smallest eigenvalue of the prior covariance  $R_2$  to check the realizability. No violation appears for both MQG-DO and QG-DO method. Finally to show the effect of adaptive resampling, we plot the effective ensemble size  $N_{\text{eff}}$  in the last row for MQG-DO and QG-DO filter with adaptive resampling as well as the QG-DO method with constant perturbation all along the process. The results show that the adaptive inflation can effectively avoid particle collapse while QG-DO method will collapse to single particle value if constant amplitude of noises is added. The inflation function (27) is also plotted on the right. Large noises are only added when particles are close to collapse.

#### 4. Applications of the blended algorithms

In this section, we test the performances of the blended particle filtering strategies developed above using the L-96 system (17) with 40 state variables. The L-96 system is designed to mimic baroclinic turbulence in the midlatitude atmosphere with the effects of energy conserving nonlinear advection and dissipation. This model has a wide variety of different chaotic regimes as the external forcing  $F$  varies, ranging from weakly chaotic to strongly chaotic to fully turbulent (see a comparison of the statistics of L-96 system in different dynamical regimes in Appendix B). The filter performances with blended methods are compared in

these various chaotic regimes with different temporal observation frequencies as well as plentiful and regularly spaced sparse spatial observations. Two dynamical regimes with quite different statistical features will be considered here; one is a weakly chaotic regime  $F = 5$  with strong non-Gaussian statistics for the leading most energetic modes and the other is a strongly chaotic regime  $F = 8$  where the statistics of every mode become almost Gaussian. We divide the numerical tests into two categories depending on the precision of forecast systems. Firstly, the filtering skill using perfect forecast system with the external forcing value  $F$  the same as that in the truth will be tested. Secondly, considering that it is always impossible to get access to the exact perfect dynamics in real applications of realistic models, it is useful to check the effects of model errors in filtering process. In this test model of L-96 system, model errors are introduced by perturbing the external forcing values away from the truth. It is interesting to check whether these methods can still preserve the skill of getting the right statistics of each mode with errors in the forecast models and how the model errors will affect the filtering results in various statistical regimes with both plentiful and regularly spaced sparse observations. We will use the forecast model with incorrect forcing  $F = 6$ , as the imperfect model for both the weakly chaotic  $F = 5$ , and strongly chaotic  $F = 8$ , regime. This is a challenging test suite for the blended filters with model error.

##### 4.1. Comparison of filter performance in various regimes

First we test the case without model error included. Two different external forcing terms ( $F = 5$ , weakly chaotic; and  $F = 8$ , strongly chaotic) of the 40-mode L-96 system will be considered here to check the performances of the methods in both Gaussian and non-Gaussian statistical regimes. With periodic boundary condition assumed and translation invariant property satisfied for the system, it is natural to study the statistics of the system in different regimes utilizing discrete Fourier modes. In weakly chaotic regime  $F = 5$ , the energy spectrum is dominated by the first several Fourier modes with wavenumbers 7, 8. The probability density functions of the first two Fourier modes appear strong non-Gaussian distributions with fat tails in steady states. The steady state single-point statistics (averaged total variance in steady state for each grid point) can be calculated as  $\bar{E}_p = 2.21$ . It takes a long time for the modes to forget their previous information, which can be measured by the absolute decorrelation time (that is, the integration over time about the absolute value of the autocorrelation function) as  $T_{\text{corr}} = 4.4$ . On the other hand, in the strongly chaotic regime  $F = 8$ , the energy spectrum becomes more homogeneous and the probability density functions of all the Fourier modes in statistical steady state are close to Gaussian. The corresponding single-point statistics and absolute decorrelation time in this regime can be measured as  $\bar{E}_p = 6.40$  and  $T_{\text{corr}} = 0.32$  respectively (see Appendix B). In the filtering process, with longer observation time step and sparser observations of the grid points, capturing the non-Gaussian features of the system becomes more crucial in getting accurate filtering results because the corrections from the observation data become less sufficient for improving the model forecasts. To compare the changes in different regimes with different observation types, observation data is taken regularly at every  $p$  grid point in the physical domain, that is, observations at  $40/p$  grid points with equal distance are taken; the case  $p = 1$  corresponds to plentiful observations and we also test cases  $p = 2, 4, 8$  of regularly spaced sparse observation with correspondingly 20, 10, 5 grid points observed compared with the full model with 40 grid points in total. The observation noises are taken to be a Gaussian white noise with variances a little more than half of the steady state single-point statistics  $\bar{E}_p$ ; specifically, we choose  $r_0 = 1.5$  for  $F = 5$  and  $r_0 = 3.5$  for  $F = 8$ . For each regime, 8

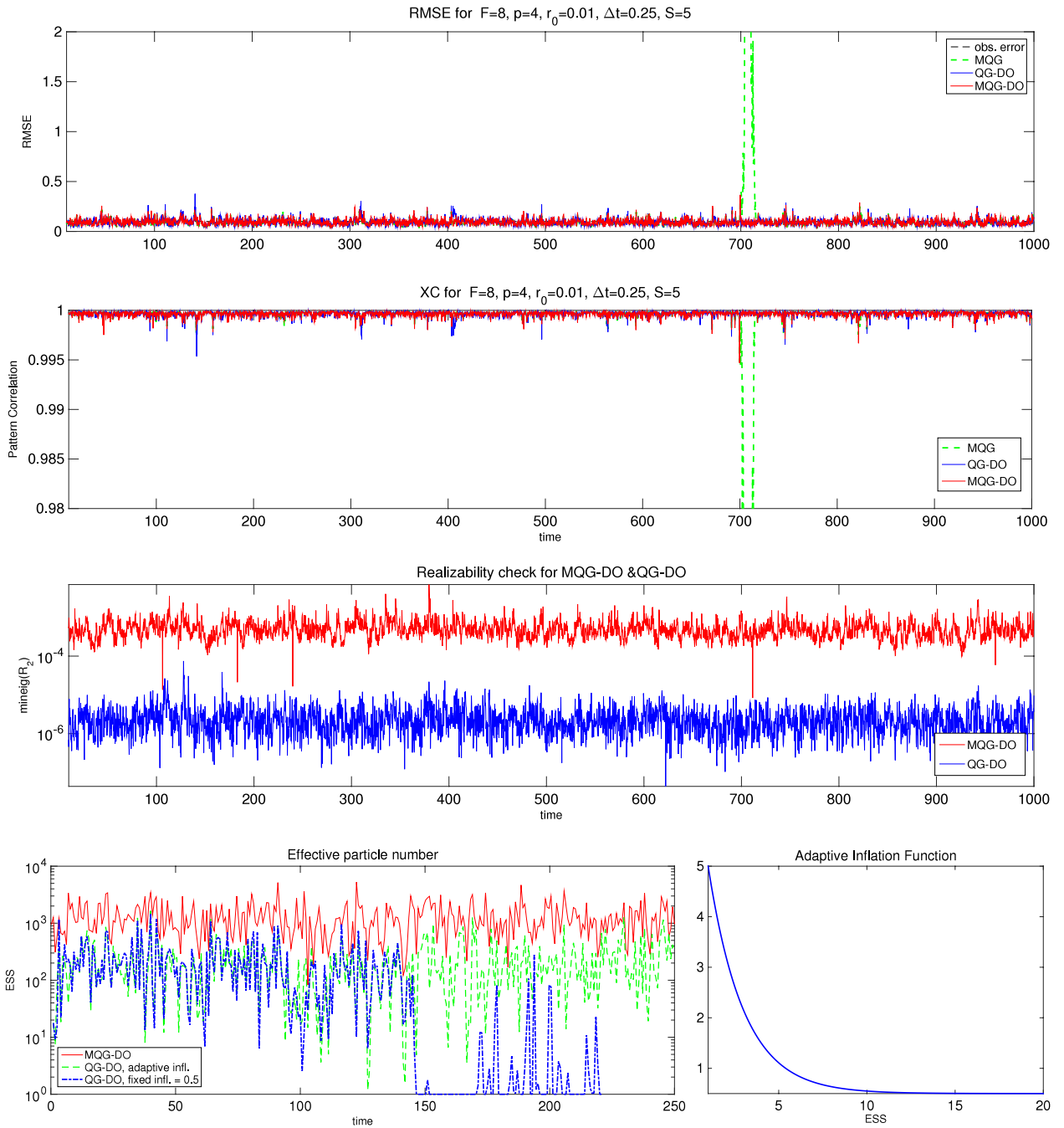


**Fig. 6.** Checking for long time stability of the schemes. The first two rows show the RMSEs and pattern correlations for MQG, QG-DO, and MQG-DO methods in a tough regime for particle methods with sparse infrequent high quality observations. The third row shows the smallest eigenvalue of the posterior matrix  $R_2$  for each method after filtering. The last row shows that adaptive inflation in the resampling process for QG-DO method can effectively avoid particle collapse and ensure stability. The corresponding particle inflation function is also plotted.

different observation time steps ranging from quite frequent times all the way to nearly the absolute decorrelation time are taken; that is,  $\Delta t = 0.2, 0.4, 0.6, 0.8, 1.0, 1.2, 1.4, 1.6, 1.8$  for  $F = 5$  and  $\Delta t = 0.04, 0.08, 0.12, 0.16, 0.20, 0.24, 0.28, 0.32$  for  $F = 8$ .

We will test the filtering performances in these two distinct dynamical regimes with the four different forecast models described in Section 2.1.2 denoted as MQG-DO filter, QG-DO filter, and MQG filter, QG filter. The first two models (MQG-DO and QG-DO filter) are the blended methods with an ensemble of particles running in a low dimensional reduced order subspace. The dimensionality of the reduced subspace is chosen to be  $s = 5$ , compared with the full dimensionality of 40 for the true L-96 system, to capture the non-Gaussian statistics inside the subspace.

Note that the number of the positive Lyapunov exponents, which reflects the dimension of the expanding subspace of the attractor, is 9 and 13 separately [26] for the two regimes  $F = 5$  and  $F = 8$ . So the five dimensional adaptive subspace with particle filtering contains at most half of the unstable directions on the attractor (this offers another explanation for why we need to consider the conditional Gaussian mixtures in the orthogonal subspace in the blended methods as described in Section 2.2.1). For all the computations following, the ensemble is chosen to contain 10,000 particles, which is large enough to capture the subspace statistics with desirable accuracy (and indeed much smaller ensemble size can be used, and the larger particle number is applied here to get rid of the random fluctuations in the comparisons for errors

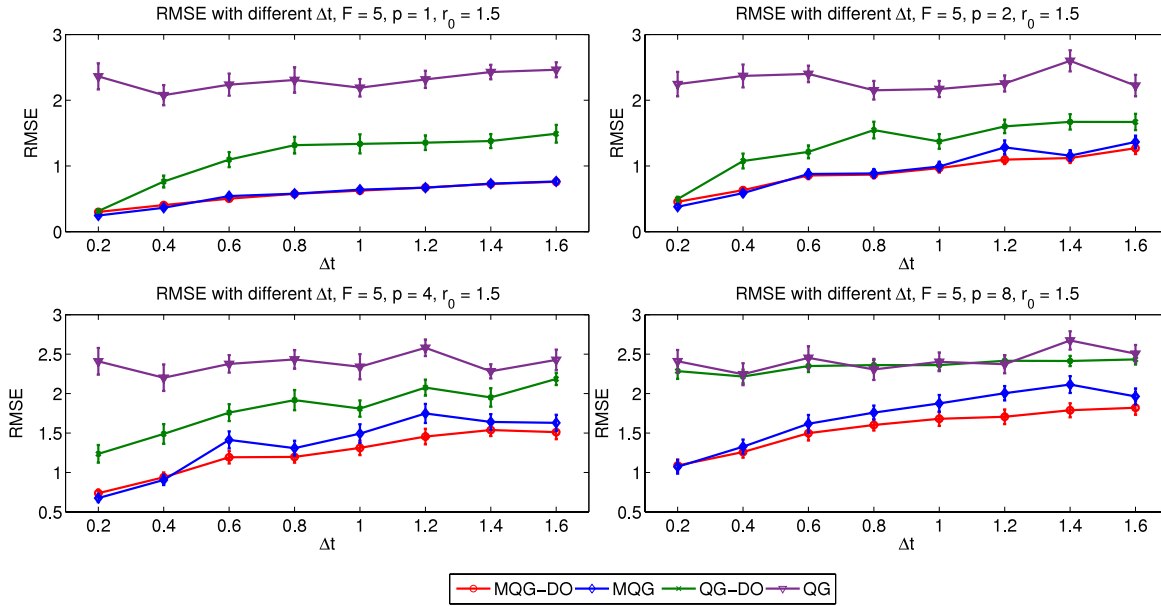


**Fig. 7.** Comparison of RMSEs in weakly chaotic regime  $F = 5$  with observation noise  $r_0 = 1.5$ . The four panels display results with different spatial observation frequencies  $p = 1, 2, 4, 8$ , and errors with increasing observation time  $\Delta t$  are compared in each panel. The error bar marks the variances of the RMS errors in time along the filtering trajectory. Blended MQG-DO method gives the best results while QG filter has the worst error.

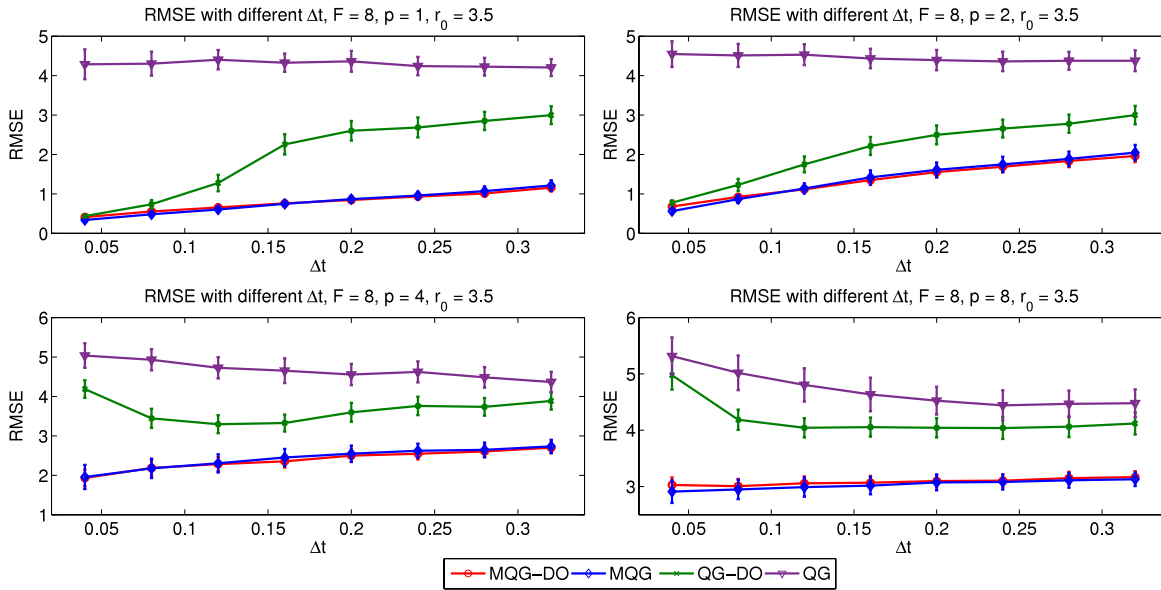


**Fig. 8.** Comparison of RMSEs in strongly chaotic regime  $F = 8$  with observation noise  $r_0 = 3.5$ . The four panels display results with different spatial observation frequencies  $p = 1, 2, 4, 8$ , and errors with increasing observation time  $\Delta t$  are compared in each panel. The error bar marks the variances of the RMS errors in time along the filtering trajectory. Blended MQG-DO method gives the best results while QG filter has the worst error.

with other factors changing). The second two methods (MQG and QG filter) are two further simplified models with only quasi-Gaussian statistics (at most including the steady state higher order moments) considered. Despite the insufficiency in accurately capturing non-Gaussian features of these closure methods, as it can be seen in the results following, the MQG method can give desirable filtering results in regimes where non-Gaussianity is not a strong factor of interest. The methods without the need of running an ensemble of particles become even more efficient in computation, making it a more feasible model for filtering real climate systems with irreducible high dimensional attractors. Finally the QG closure method with all higher order statistics neglected is compared to emphasize the role of higher order moments in improving filtering performances.

In Figs. 7 and 8, the RMS errors with various observation steps as well as plentiful and sparse spatial observations are compared for regime  $F = 5$  and  $F = 8$  separately. Along with each RMSE plotted, one errorbar is added at each test point to measure the variance of the errors in time along the long trajectory in the realization. The introduction of these variances in error is to measure the stability features of these methods. For two filtering methods with similar amplitude of the time averaged RMSEs, the temporal evolution of the errors in time may have either large deviations from the mean or keep staying close to the time averaged value. So larger variance in the error indicates higher possibility of filter divergence and weaker robustness of the method. For both regimes, the blended MQG-DO filter maintains good performance with minimum RMSEs among all the methods tested. In the near Gaussian regime  $F = 8$

and in non-Gaussian regime  $F = 5$  with frequent spatial and temporal observations where non-Gaussian effect is not a central issue, the MQG filter has similar filtering ability compared with MQG-DO filter. This shows the advantage of MQG filter in Gaussian regimes considering its higher efficiency. As the non-Gaussian features become gradually important in regime  $F = 5$  with sparse observations or long observation steps, capturing the true statistics with accuracy becomes more crucial for improving filtering results, and MQG filter appears inferior with larger error compared with MQG-DO filter. MQG filter also gets larger variances in the error (from the errorbars) even with similar time averaged RMS errors, showing weaker stability compared with MQG-DO filter. The QG-DO filter works fine with small observation steps and plentiful or not too sparse spatial observations whereas the error grows larger with sparser and less frequent observations. The QG filter ignores all the higher order moments in the dynamics, thus fails to filter the system uniformly in all regimes. This offers another example to show the importance of higher order statistics in successfully filtering the system. For more tests on non-Gaussian filter performance in the perfect model setting, see [19].

#### 4.2. Filtering performance with model error

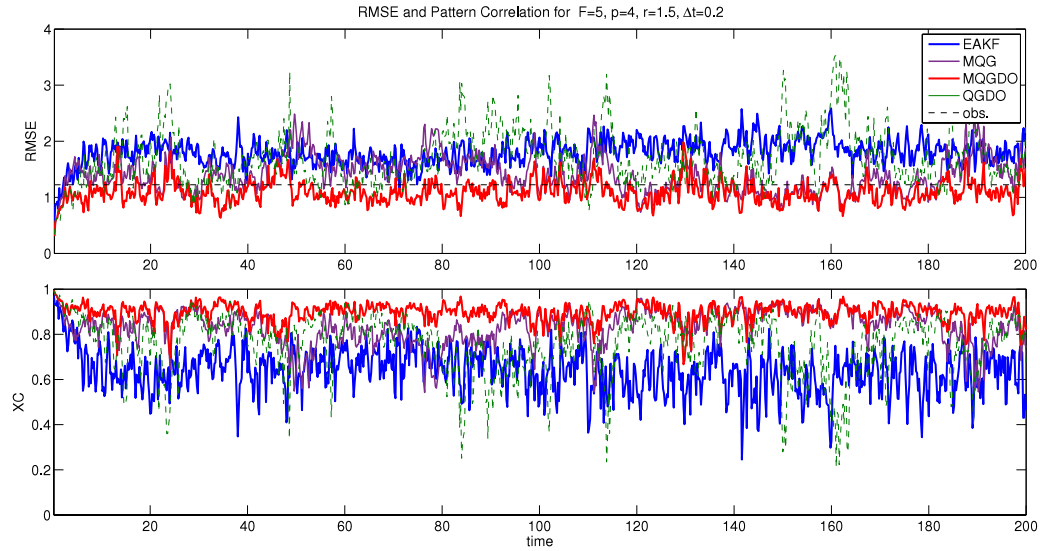
In the above, we compare extensively the filter performances of different filtering methods in different dynamical regimes with various types of observations. There all the computations are carried out under the assumption that the exact dynamics of the system are known. However a central issue in practical filtering of turbulent signals is the inclusion of model error, since the perfect system is always not available in practical applications considering the complexities in both modeling and computation of the high dimensional turbulent system. Keeping this in mind, it is useful here to test the performance of these filtering methods in the appearance of model errors using the simpler L-96 system in the first place. There exist different sources for model errors, driving the imperfect model solution away from the true dynamics of the system to another regime. Since the dynamical regimes of the L-96 system change with different values of external forcings, one simple and effective way to simulate model error in L-96 model is to perturb the external forcing away from its original value. In our test cases here, we still get the truth from two typical dynamical regimes with  $F = 5$  and  $F = 8$ , while imperfect model error will be introduced to the system by setting  $F = 6$  for the forecast models in both cases. Therefore, we will check the models' ability to filter the signals in two distinct regimes  $F = 5, 8$  using the same forecast dynamical model with imprecise predictions from  $F = 6$ . As can be seen in Appendix B, the steady state statistics with  $F = 6$  become quite close to Gaussian distributions. Thus, the model errors for the Gaussian regime,  $F = 8$ , occur through the different energetics in the imperfect forecast model. Whereas considering the highly non-Gaussian features of the regime  $F = 5$ , it is a difficult test to apply these imperfect models with near Gaussian statistics to capture the non-Gaussian statistics in this regime.

We will test the filter performances with model error  $F = 6$  in the two regimes  $F = 5, 8$  with moderate observation noise and observation time step, that is,  $r_0 = 1.5$ ,  $\Delta t = 0.2$  for  $F = 5$  and  $r_0 = 3.5$ ,  $\Delta t = 0.12$  for  $F = 8$ . The blended MQG-DO and QG-DO filter as well as the Gaussian MQG filter with model error included in the forecast model will be tested. The setup for these methods is the same as the previous case without model error. For comparison, we also include the results from the ensemble adjustment Kalman filter (EAKF) with inflation and localization with 100 ensemble members (no significant change occurred with larger ensemble sizes) [8,9]. EAKF works well with a relatively smaller ensemble size by adjusting the posterior particle values close to the hyper-plane where prior results locate. However in the

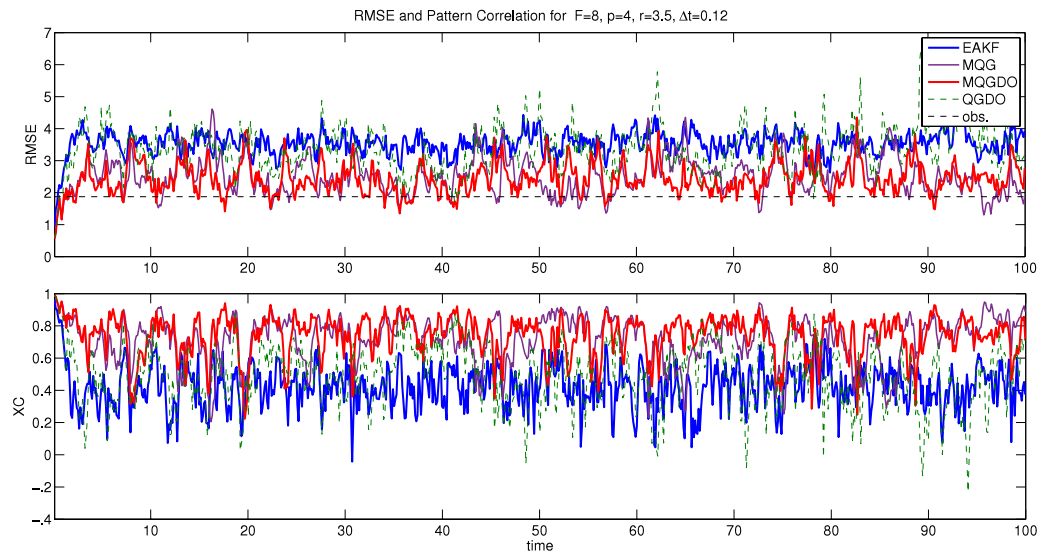
present case with model error in the forecast model, adjustments of particles to the prior distribution with wrong statistics may not be good for accurate filtering. To avoid this over-emphasis about an inaccurate prior distribution, a relatively larger inflation factor is added for the EAKF method in order to make sure the filter solutions do not diverge from the observations in the inaccurate model forecasts. Thus we choose inflation factor 1.4 and localization factor 0.2 throughout the cases.

In Fig. 9 we compare the RMS errors and pattern correlations between the posterior mean and the truth in the two dynamical regimes with regularly spaced sparse observations  $p = 4$ . The RMS errors for the MQG-DO filter stay low in comparable amplitude with the observation noise considering only 1/4 of the grid points observed. The MQG filter is only a little worse and it performs better in the near Gaussian regime  $F = 8$  than that in the non-Gaussian regime  $F = 5$  due to its errors in estimating the higher order moments. For the QG-DO method, it becomes less stable here with model error introduced since it uses the inaccurate dynamics in the forecast model without steady state corrections like the MQG-DO and MQG methods. The EAKF method is stable but has larger errors in the filtering results. For further comparisons, we list the time averaged RMS errors and pattern correlations with these methods in Table 2. Both plentiful ( $p = 1$ ) and three regularly spaced sparse observation networks ( $p = 2, 4, 8$ ) are compared. In addition, to display the effect of model errors, we also list the RMS errors and pattern correlations for MQG-DO filter results using perfect system without model error. Due to the near Gaussian statistics of the imperfect model with  $F = 6$ , the imperfect model does not diminish the filter performance much in regime  $F = 8$ . On the other hand, in regime  $F = 5$ , the imperfect forecast models with near Gaussian statistics show large deficiency in filtering results compared with the perfect model results. But MQG-DO remains quite skillful even with this severe model error.

Finally, it is also useful to check the methods' ability to capture the right statistical distributions of the true system. The accuracy of the filtering results always relies on forecast models' skill to obtain the right statistics. Due to the ergodicity of the L-96 system in both regimes, the pdfs of the modes with both blended methods and EAKF can be achieved by running an ensemble of simulations in statistical steady state for a long time. Large ensemble size will be applied here to get smoother distributions. We have already compared the pdfs achieved through different filtering methods with the perfect model in our previous paper [19]. Further here in Fig. 10, the distributions using methods with model error included are plotted. First the forecast pdfs for the absolute values of the first most energetic Fourier modes ( $|\hat{u}_7|$  for  $F = 5$  and  $|\hat{u}_8|$  for  $F = 8$ ) are compared. The absolute value of a Gaussian random variable will appear as a Rayleigh distribution as shown in the pdfs of EAKF method. In regime  $F = 5$ , even with the imperfect forecast model, the structure of non-Gaussianity of the first mode can still be captured by MQG-DO method. MQG method gives less accurate estimation whereas QG-DO method becomes poor in getting the non-Gaussian features since no higher order statistics are considered in this method. On the other hand, in the regime  $F = 8$ , all the results appear more Gaussian. Still MQG-DO can have a much more accurate characterization of the true distribution whereas EAKF results have much wider spread. Besides the forecast distributions, we also compare the pdfs for the forecast error, that is, the distribution from the difference of the model prior and the truth  $\hat{u}_{k,model} - \hat{u}_{k,truth}$ . Tighter distributions in the forecast error show better skill in predicting the truth with these filtering methods. As shown in both cases, MQG-DO method gets the tightest pdfs for the error, while EAKF has the largest forecast error spread. At last, to measure the influence of model errors in filter performance, we plot the same pdfs using MQG-DO method with and without model errors in Fig. 11. In regime  $F = 5$ ,



(a)  $F = 5$ .



(b)  $F = 8$ .

**Fig. 9.** Comparison of RMSEs and pattern correlations between methods with model error  $F = 6$  in the forecast model. The upper panel is the results in regime  $F = 5$  with parameters  $r_0 = 1.5$ ,  $\Delta t = 0.2$ ,  $p = 4$ ; the lower panel is the result in regime  $F = 8$  with parameters  $r_0 = 3.5$ ,  $\Delta t = 0.12$ ,  $p = 4$ .

**Table 2**  
Comparison of RMSEs and pattern correlations (XC) through different filtering methods with model error. Full ( $p = 1$ ) and regularly sparse ( $p = 2, 4, 8$ ) observations are both tested in the two different dynamical regimes  $F = 5$  and  $F = 8$  with observation noises and observation time step  $r_0 = 1.5$ ,  $\Delta t = 0.2$  and  $r_0 = 3.5$ ,  $\Delta t = 0.12$  respectively. The model error is introduced by setting  $F = 6$  in the imperfect forecast model for both regimes. The last column shows the MQG-DO filter results without model error in the forecast model for comparison.

$p$	MQG-DO		MQG		QG-DO		EAKF		MQG-DO w/o ME	
	RMSE	XC	RMSE	XC	RMSE	XC	RMSE	XC	RMSE	XC
(a) $F = 5, r_0 = 1.5, \Delta t = 0.2$										
1	0.8134	0.9536	0.6001	0.9756	1.1594	0.9075	0.6694	0.9677	0.3009	0.9919
2	0.8478	0.9466	0.8546	0.9428	1.3914	0.8649	0.8790	0.9390	0.4552	0.9814
4	1.1136	0.8968	1.4417	0.8353	1.7675	0.7685	1.8242	0.6420	0.7369	0.9508
8	1.5175	0.7895	1.5391	0.7745	2.3525	0.4238	2.2212	0.3908	1.0890	0.8899
(b) $F = 8, r_0 = 3.5, \Delta t = 0.12$										
1	1.1025	0.9611	0.9153	0.9717	1.4660	0.9224	1.3136	0.9411	0.6541	0.9840
2	1.3991	0.9310	1.5276	0.9116	2.0987	0.8314	1.7584	0.8843	1.1142	0.9528
4	2.4786	0.7481	2.5658	0.7286	3.4275	0.5201	3.5725	0.4359	2.2832	0.7889
8	3.0687	0.5538	3.0985	0.5494	4.0680	0.2695	21.7222	0.1711	3.0578	0.5599

the filter’s prediction for forecast statistics becomes more accurate and the non-Gaussian structure can be captured with accuracy by MQG-DO method if perfect model is applied. In regime  $F = 8$ , also

perfect agreement can be seen from the MQG-DO result without model error. Furthermore, by comparing the pdfs of forecast errors, tight distributions with little degeneracy can be seen even with

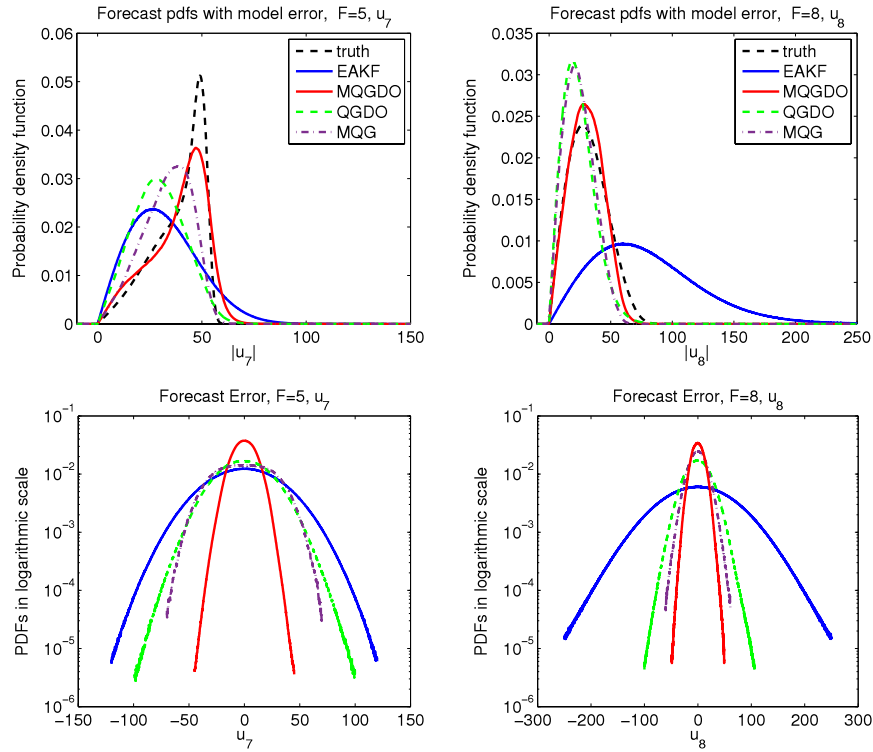


**Fig. 10.** Comparison of the statistics of the leading Fourier mode ( $\hat{u}_7$  for  $F = 5$  and  $\hat{u}_8$  for  $F = 8$ ) in regimes  $F = 5, 8$  captured through MQG-DO, QG-DO, MQG, and EAKF filters with imperfect model error  $F = 6$ . The first row shows the forecast pdfs of absolute values of the modes captured by different methods compared with the truth from Monte-Carlo simulations in black dashed lines. The second row is the pdfs for the forecast error  $\hat{u}_{j,\text{model}} - u_{j,\text{truth}}$  captured with different filtering methods.

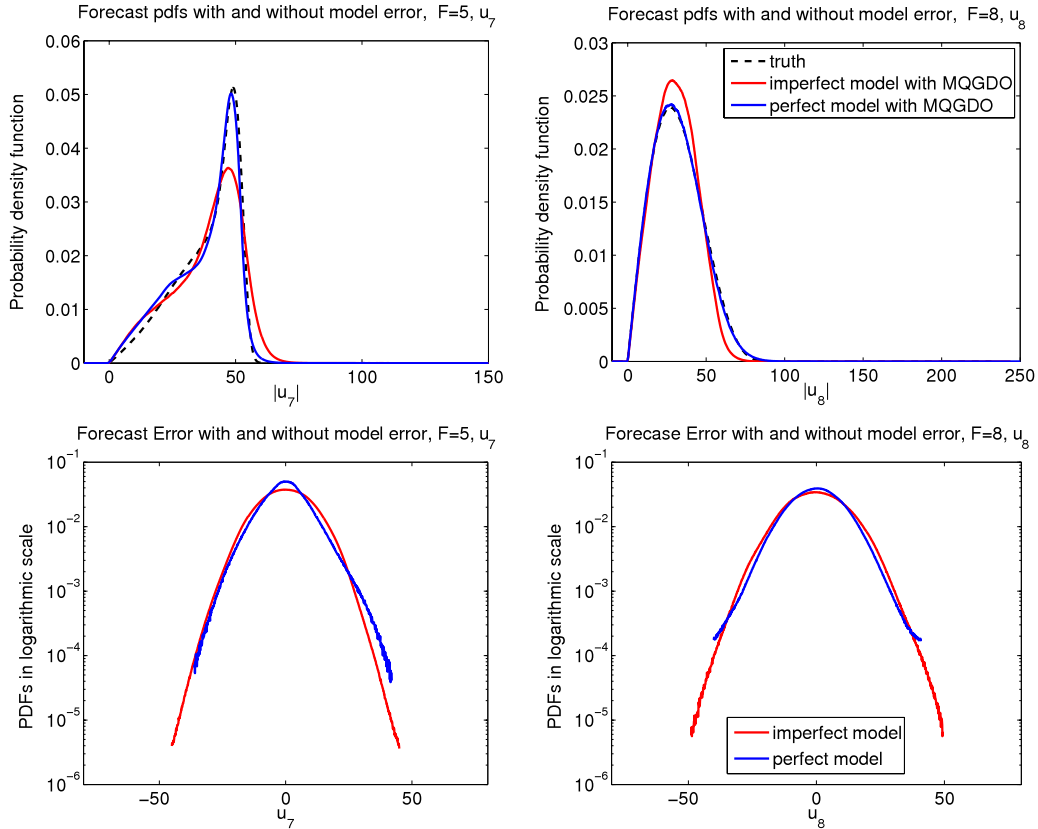


**Fig. 11.** Comparison of principal mode statistics achieved through imperfect model with model error (using  $F = 6$ ) and perfect model without model error (using the true  $F$ ) in regimes  $F = 5, 8$ . The forecast pdfs for the leading mode (first row) and the forecast error pdfs (second row) as in Fig. 10 using MQG-DO filter are compared. Without including model errors, more accurate pdfs for the mode are captured by the filter while tight distributions for the forecast errors are achieved in both cases with and without model errors.

the case including model error, showing the high prediction skill of the MQG-DO combined filtering prediction system even with the imperfect model forecasts using  $F = 6$  both for the weakly chaotic,  $F = 5$ , and strongly chaotic,  $F = 8$ , regimes.

## 5. Concluding discussion

In this paper, we offer extensive description and discussion for the blended particle filters introduced in [19]. The basic idea for this method is to capture non-Gaussian features in an adaptively evolving low dimensional subspace through particles interacting with evolving Gaussian statistics on the remaining phase space. It is shown by simple examples that both the ideas about evolving low dimensional subspaces and conditional Gaussian distribution in the orthogonal part are essential for the effectiveness and accuracy of filtering results. The performances of the filtering methods are compared in various dynamical regimes with different statistical features using the forty dimensional L-96 system with only a five dimensional subspace for nonlinear particle filter. The effect of model error for filter performance is also checked by adding perturbations to the external forcing term of the system. Over the various dynamical regimes with changing statistics and in the presence of distinct statistical errors introduced by imperfect models, the blended filtering methods demonstrate uniform high skill in both capturing important non-Gaussian dynamical features and achieving accurate filtering results in various regimes and different kinds of observation data.

The blended filtering methods here also show potential to be applied to more generalized realistic problems. Our focus above is majorly about the development of the blended filtering scheme and displaying the performance using simple models in the first place. Still, to apply the methods to more realistic models, several further difficulties need to be considered. As pointed out by one of the reviewers, it is useful to check the filter performance with varying DO subspace dimensionality  $s$  and develop a judicious way to determine its value. This is related with the development of proper reduced order uncertainty quantification models. For example, the low-order models in [35] offer a promising way to run forecast system with efficiency. It is also useful to check the blended filter responds to decreasing ensemble size in the low dimensional subspace. In this paper, we use unnecessarily large ensemble size to guarantee particle filter convergence and to estimate the filter distributions. Effects with smaller particle numbers need to be checked for practical applications. Especially it is another independent research topic to investigate proper resampling strategies for particle filters with limited number of particles to avoid particle collapse. These are the possible directions for further developments of the methods.

## Acknowledgments

The research of Andrew Majda is partially supported by MURI grant 25-74200-F7112 where Di Qi is supported as a graduate research assistant. The authors thank Nan Chen for helpful discussions. The authors also thank the two anonymous reviewers who both offer valuable comments and suggestions.

## Appendix A. Exact solution for the $2 \times 2$ non-normal linear system

The linear system that is tested in Section 2.2 is a two dimensional system with variables  $\mathbf{x} = (x, y)$  as a standard Ornstein–Uhlenbeck process. The dynamics of  $x$  is a deterministic process while stochasticity is only introduced by variable  $y$  so that

$$d\mathbf{x} = A\mathbf{x}dt + \Sigma d\mathbf{W}_t, \quad (\text{A.1})$$

with

$$A = \begin{bmatrix} -a & \epsilon_1 \\ \epsilon_2 & -b \end{bmatrix}, \quad \Sigma = \begin{bmatrix} 0 & 0 \\ 0 & \sigma \end{bmatrix}.$$

$\lambda_{1,2} = -\frac{1}{2}(a+b) \pm \frac{1}{2}[(a-b)^2 + 4\epsilon_1\epsilon_2]^{\frac{1}{2}}$  are the eigenvalues of  $A$ . The non-normal features are characterized by the non-commutability of  $A$  and  $A^*$ . If we calculate the eigenvectors of  $A$ ,  $\mathbf{v}_1 = (\epsilon_1, a + \lambda_1)^T$ ,  $\mathbf{v}_2 = (b + \lambda_2, \epsilon_2)^T$ , they cannot be orthogonal to each other under the non-normal assumption  $\epsilon_1 \gg 1$ , and  $\epsilon_2 = 0$ . Also note that in this extreme regime, the angle between the eigenvectors is sensitive to the variation of  $a$  but only one of the eigenvectors  $\mathbf{v}_1$  changes its orientation as  $a$  changes.

The exact analytic solution of the above system can be expressed as

$$\begin{pmatrix} x \\ y \end{pmatrix} = e^{A(t-t_0)} \begin{pmatrix} x_0 \\ y_0 \end{pmatrix} + \int_{t_0}^t e^{A(t-s)} \Sigma dW_s. \quad (\text{A.2})$$

The solution is always a Gaussian distribution as long as the initial value is Gaussian. Then only the first and second order moments are required to get the full distribution of the solutions

$$\begin{pmatrix} \bar{x} \\ \bar{y} \end{pmatrix} = e^{A(t-t_0)} \begin{pmatrix} x_0 \\ y_0 \end{pmatrix}, \quad (\text{A.3})$$

$$R(t, t_0) = e^{A(t-t_0)} R_0 e^{A^T(t-t_0)} + \int_{t_0}^t e^{A(t-s)} \begin{pmatrix} 0 & 0 \\ 0 & \sigma^2 \end{pmatrix} e^{A^T(t-s)} ds. \quad (\text{A.4})$$

By only considering the dynamics in the principal direction as the reduced order method described in Section 2.1, take  $\mathbf{x} = u_1 \mathbf{e}_1(t)$ , with  $\mathbf{e}_1(t)$  getting the direction with largest variance through (A.4). To run the forecast model using QG-DO method, the dynamics for the basis and stochastic coefficients need to be calculated. For this two-dimensional system, the dynamical basis  $\mathbf{e}_1(t)$  can be determined by its angle  $\theta$  with the axis, that is,  $\mathbf{e}_1(t) = (\sin \theta(t), \cos \theta(t))^T$ . Substitute  $\mathbf{e}_1$  and  $u_1$  into the standard DO equations for basis (15) and coefficients (14), we find

$$\frac{d\mathbf{e}_1}{dt} = A\mathbf{e}_1 - (\mathbf{e}_1^T A \mathbf{e}_1) \mathbf{e}_1,$$

$$\frac{du_1}{dt} = (\mathbf{e}_1^T A \mathbf{e}_1) u_1 + \sigma \dot{W} \cdot \mathbf{e}_1.$$

After some calculation, the equations for the DO direction  $\theta$  and stochastic coefficients  $u_1$  are achieved as

$$\frac{d\theta}{dt} = (b-a) \sin \theta \cos \theta + \epsilon_1 \cos^2 \theta - \epsilon_2 \sin^2 \theta, \quad (\text{A.5})$$

$$\frac{du_1}{dt} = (-a \sin^2 \theta - b \cos^2 \theta + (\epsilon_1 + \epsilon_2) \sin \theta \cos \theta) u_1 + \sigma \cos \theta \dot{W}. \quad (\text{A.6})$$

Then it is easy to reach the dynamics of the covariance  $C_{u_1 u_1}$  of the stochastic coefficient

$$\frac{dC_{u_1 u_1}}{dt} = -2(a \sin^2 \theta + b \cos^2 \theta - (\epsilon_1 + \epsilon_2) \sin \theta \cos \theta) C_{u_1 u_1}(t) + \sigma^2 \cos^2 \theta. \quad (\text{A.7})$$

Therefore all the equations required for the reduced order methods are achieved here with exact forms. The exact solutions of the mean and covariance matrix can be calculated at every time instant. The DO direction  $\theta$  can be achieved by integrating equation (A.5) with high-order scheme. Then fixing  $\theta$  at each time instant, the dynamical stochastic equation of  $u_1$  is also easy to get through Monte–Carlo simulation, with small integration step required to guarantee the accuracy of the random process. The accuracy of

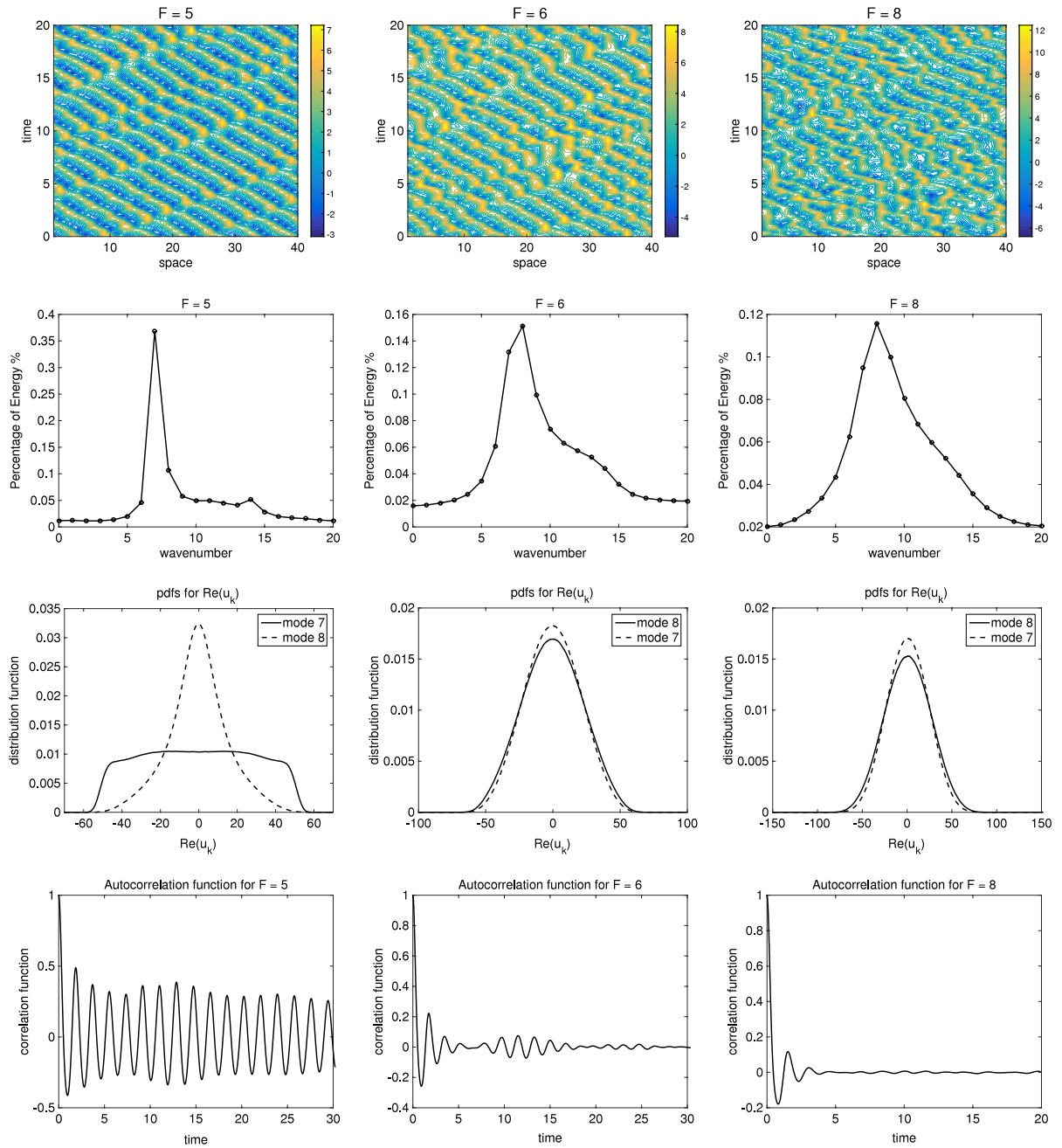


**Fig. B.12.** Summary of statistics for the L-96 system: time series of the 40 state variables of L-96 system in various regimes (first row); energy spectra in Fourier space (second row); the pdfs for the first two principal Fourier modes (third row); and the autocorrelation functions of the state variable (fourth row). Regimes for weakly chaotic ( $F = 5$ , left), chaotic ( $F = 6$ , middle), and strongly chaotic ( $F = 8$ , right) dynamics are compared.

the approximation of  $u_1$  can also be checked by the solution of  $C_{u_1 u_1}$  in (A.7). In this way, we can assume that no system error is introduced in the resolved direction during the forecast step. A clean output for the prior distribution can be achieved. This helps us focus on the errors from the DO decomposition and the analysis step.

## Appendix B. Statistics of the L-96 system in various regimes

The major test model in this paper is the L-96 model which is a 40-dimensional nonlinear chaotic dynamical system mimicking the large-scale behavior of the mid-latitude atmosphere. It can be

formulated as

$$\frac{du_j}{dt} = u_{j-1}(u_{j+1} - u_{j-2}) - u_j + F, \quad j = 0, \dots, J-1 \quad (\text{B.1})$$

with  $J = 40$  and  $F$  the deterministic forcing parameter. We test the filter performances in both weakly chaotic regime ( $F = 5$ ) and strongly chaotic regime ( $F = 8$ ), and the imperfect model with model error is in the chaotic regime ( $F = 6$ ). The statistics for these three cases are shown in Fig. B.12. Strong non-Gaussian statistics can be seen from the weakly chaotic regime  $F = 5$  while near Gaussian distribution is shown in strongly chaotic regime  $F = 8$ , and  $F = 6$  shows the statistics in between.

To characterize the chaoticity in each regime, it is also useful to introduce the pointwise energy at each grid point  $\bar{E}_p$  and the

absolute decorrelation time  $T_{\text{corr}}$ . Using ergodicity of the system, the pointwise energy can be defined as the temporal mean of the fluctuations along one trajectory

$$\bar{E}_p = \lim_{T \rightarrow \infty} \frac{1}{T} \sum_{j=0}^{J-1} \frac{1}{J} \int_{T_0}^{T_0+T} (u_j(t) - \bar{u})^2 dt,$$

with  $\bar{u} = \lim_{T \rightarrow \infty} \frac{1}{T} \int_{T_0}^{T_0+T} u_j(t) dt$  the temporal mean. The absolute decorrelation time can be defined as the integration of the absolute value of the autocorrelation function

$$T_{\text{corr}} = \int_0^\infty \left| \frac{\langle (u_j(t) - \bar{u})(u_j(t + \tau) - \bar{u}) \rangle_t}{\langle (u_j(t) - \bar{u})^2 \rangle_t} \right| d\tau.$$

### Appendix C. Solving the variational problem for the most probable conditional distribution

The maximum-entropy problem in Section 3.1 can be rephrased as to find the distribution  $p^* = p^*(\mathbf{u}_2|\mathbf{u}_1)$ , such that,

$$p^*(\mathbf{u}_2|\mathbf{u}_1) = \operatorname{argmax}_{p \in \mathcal{C}} \int p_-(\mathbf{u}_1) \delta [p(\mathbf{u}_2|\mathbf{u}_1)] d\mathbf{u}_1, \quad (\text{C.1})$$

under the conditions  $\mathcal{C}$ :

$$p(\mathbf{u}_2|\mathbf{u}_1) \geq 0, \quad \int p(\mathbf{u}_2|\mathbf{u}_1) d\mathbf{u}_2 = 1, \quad \forall \mathbf{u}_1, \quad (\text{C.2a})$$

$$\bar{\mathbf{u}}_2^- = \iint \mathbf{u}_2 p_-(\mathbf{u}_1) p(\mathbf{u}_2|\mathbf{u}_1) d\mathbf{u}_1 d\mathbf{u}_2, \quad (\text{C.2b})$$

$$R_{12} = \iint (\mathbf{u}_1 - \bar{\mathbf{u}}_1^-) \otimes (\mathbf{u}_2 - \bar{\mathbf{u}}_2^-) \times p_-(\mathbf{u}_1) p(\mathbf{u}_2|\mathbf{u}_1) d\mathbf{u}_1 d\mathbf{u}_2, \quad (\text{C.2c})$$

$$R_2 = \iint (\mathbf{u}_2 - \bar{\mathbf{u}}_2^-) \otimes (\mathbf{u}_2 - \bar{\mathbf{u}}_2^-) \times p_-(\mathbf{u}_1) p(\mathbf{u}_2|\mathbf{u}_1) d\mathbf{u}_1 d\mathbf{u}_2. \quad (\text{C.2d})$$

The first constraint is to make sure that the optimization result is still a density function and the following three constraints guarantee the consistency with prior statistics in mean and covariance.

Denoting  $p \equiv p(\mathbf{u}_2|\mathbf{u}_1)$ , a standard variation about the entropy function  $S$  as well as the constraints  $\mathcal{C}$  gives

$$\frac{\delta \delta}{\delta p} = -(1 + \log p) p_-(\mathbf{u}_1),$$

$$\frac{\delta \bar{\mathbf{u}}_2^-}{\delta p} = \mathbf{u}_2 p_-(\mathbf{u}_1),$$

$$\frac{\delta R_{12}}{\delta p} = (\mathbf{u}_1 - \bar{\mathbf{u}}_1^-) \otimes (\mathbf{u}_2 - \bar{\mathbf{u}}_2^-) p_-(\mathbf{u}_1),$$

$$\frac{\delta R_2}{\delta p} = (\mathbf{u}_2 - \bar{\mathbf{u}}_2^-) \otimes (\mathbf{u}_2 - \bar{\mathbf{u}}_2^-) p_-(\mathbf{u}_1).$$

Using all these variations, introduce Lagrangian multipliers  $\mu_0, \mu_1, \mu_2, \mu_3$ , then the optimal solution satisfies

$$\frac{\delta \delta}{\delta p} = -\mu_0 - \mu_1 \frac{\delta \bar{\mathbf{u}}_2^-}{\delta p} - \mu_2 \frac{\delta R_{12}}{\delta p} - \mu_3 \frac{\delta R_2}{\delta p}.$$

Rearrange the equation with Lagrangian multipliers above, the optimal solution can be rewritten in a compact form as

$$\log p^*(\mathbf{u}_2|\mathbf{u}_1) + \sum_{\alpha_1, \alpha_2} \mu_{\alpha_1, \alpha_2} \mathbf{u}_1^{\alpha_1} \mathbf{u}_2^{\alpha_2} + C_\alpha(\mathbf{u}_1) = 0, \quad (\text{C.3})$$

with summation index  $\{\alpha_1, \alpha_2\}$  taking over  $1 \leq |\alpha_2| \leq 2, |\alpha_1| + |\alpha_2| \leq 2$ .

The next step is to determine the Lagrangian multipliers in this equation by substituting the optimal distribution found in (C.3) back to the constraints  $\mathcal{C}$ . From (C.3), it is clear that the exponent of  $p^*$  is only a quadratic function of  $\mathbf{u}_2$ . It infers that the most probable distribution is simply Gaussian, thus only the mean and covariance matrix need to be determined. Write the Gaussian distribution abstractly as

$$p^*(\mathbf{u}_2|\mathbf{u}_1) \propto \exp\left(-\frac{1}{2}(\mathbf{u}_2 - \mathbf{m}(\mathbf{u}_1))^T (R_2^-(\mathbf{u}_1))^{-1} (\mathbf{u}_2 - \mathbf{m}(\mathbf{u}_1))\right),$$

with  $\mathbf{m}(\mathbf{u}_1)$  and  $R_2^-(\mathbf{u}_1)$  as the conditional mean and covariance of the conditional distribution. Note again in (C.3), the square term  $\mathbf{u}_2^2$  only has constant coefficient, which means constant covariance matrix  $R_2^-$  in the optimal density function  $p^*$ . Substitute  $p^*$  into (C.2b), a direct calculation gives

$$\mathbf{m}(\mathbf{u}_1) = \bar{\mathbf{u}}_2^-(\mathbf{u}_1). \quad (\text{C.4})$$

Then define

$$R_2^-(\mathbf{u}_1) \equiv \int (\mathbf{u}_2 - \bar{\mathbf{u}}_2^-(\mathbf{u}_1)) \otimes (\mathbf{u}_2 - \bar{\mathbf{u}}_2^-(\mathbf{u}_1))^T p^*(\mathbf{u}_2|\mathbf{u}_1) d\mathbf{u}_2 = R_2^-, \quad (\text{C.5})$$

independent of the choice of  $\mathbf{u}_1$ . Combining (C.5) and (C.2d), simple calculations give

$$R_2 + \bar{\mathbf{u}}_2^- \otimes \bar{\mathbf{u}}_2^- = \int \mathbf{u}_2 \otimes \mathbf{u}_2 p_-(\mathbf{u}_1) p^*(\mathbf{u}_2|\mathbf{u}_1) d\mathbf{u}_2 d\mathbf{u}_1 = R_2^- + \int \bar{\mathbf{u}}_2^-(\mathbf{u}_1) \otimes \bar{\mathbf{u}}_2^-(\mathbf{u}_1) p_-(\mathbf{u}_1) d\mathbf{u}_1.$$

Therefore we get the form for the covariance matrix

$$\begin{aligned} R_2^- &= R_2 + \bar{\mathbf{u}}_2^- \otimes \bar{\mathbf{u}}_2^- - \int \bar{\mathbf{u}}_2^-(\mathbf{u}_1) \otimes \bar{\mathbf{u}}_2^-(\mathbf{u}_1) p_-(\mathbf{u}_1) d\mathbf{u}_1 \\ &= R_2 - \int \bar{\mathbf{u}}_2'(\mathbf{u}_1) \otimes \bar{\mathbf{u}}_2'(\mathbf{u}_1) p_-(\mathbf{u}_1) d\mathbf{u}_1, \\ &= R_2 - \sum_j \bar{\mathbf{u}}_{2,j}' \otimes \bar{\mathbf{u}}_{2,j}' p_{j,-}, \end{aligned} \quad (\text{C.6})$$

with  $\bar{\mathbf{u}}_2'(\mathbf{u}_1) = \bar{\mathbf{u}}_2^-(\mathbf{u}_1) - \langle \mathbf{u}_2 \rangle$ . The last line of the above equation uses the previous discrete particle representation  $p_-(\mathbf{u}_1) = \sum_j p_{j,-} \delta(\mathbf{u}_1 - \mathbf{u}_{1,j})$ .

### References

- [1] A. Bain, D. Crisan, *Fundamentals of stochastic filtering*, in: *Stochastic Modelling and Applied Probability*, Vol. 60, Springer, New York, 2009.
- [2] A. Doucet, S. Godsill, C. Andrieu, On sequential monte carlo sampling methods for Bayesian filtering, *Statist. Comput.* 10 (3) (2000) 197–208.
- [3] B. Anderson, J. Moore, *Optimal Filtering*, Prentice-Hall, Englewood Cliffs, NJ, 1979.
- [4] T. Bengtsson, P. Bickel, B. Li, Curse-of-dimensionality revisited: collapse of the particle filter in very large scale systems, in: *Probability and Statistics: Essays in Honor of David A. Freedman 2*, 2008, pp. 316–334.
- [5] P. Bickel, B. Li, T. Bengtsson, Sharp failure rates for the bootstrap particle filter in high dimensions, in: *IMS Collections: Pushing the Limits of Contemporary Statistics: Contributions in Honor of Jayanta K. Ghosh 3*, 2008, pp. 318–329.
- [6] G. Evensen, The ensemble Kalman filter: theoretical formulation and practical implementation, *Ocean Dynam.* 53 (4) (2003) 343–367.
- [7] C.H. Bishop, B.J. Etherton, S.J. Majumdar, Adaptive sampling with the ensemble transform Kalman filter. part i: theoretical aspects, *Mon. Weather Rev.* 129 (3) (2001) 420–436.
- [8] J.L. Anderson, An ensemble adjustment Kalman filter for data assimilation, *Mon. Weather Rev.* 129 (12) (2001) 2884–2903.
- [9] J.L. Anderson, A local least squares framework for ensemble filtering, *Mon. Weather Rev.* 131 (4) (2003) 634–642.
- [10] M. Ghil, P. Malanotte-Rizzoli, Data assimilation in meteorology and oceanography, *Adv. Geophys.* 33 (1991) 141–266.

- [11] A.J. Chorin, P. Krause, Dimensional reduction for a Bayesian filter, *Proc. Natl. Acad. Sci. USA* 101 (42) (2004) 15013–15017.
- [12] B.F. Farrell, P.J. Ioannou, State estimation using a reduced-order Kalman filter, *J. Atmospheric Sci.* 58 (23) (2001) 3666–3680.
- [13] P.J. Van Leeuwen, Particle filtering in geophysical systems, *Mon. Weather Rev.* 137 (12) (2009) 4089–4114.
- [14] L.M. Berliner, R.F. Milliff, C.K. Wikle, Bayesian hierarchical modeling of air-sea interaction, *J. Geophys. Res. Oceans* 108 (C4) (2003) 3104–3120. (1978–2012).
- [15] P.F. Lermusiaux, Uncertainty estimation and prediction for interdisciplinary ocean dynamics, *J. Comput. Phys.* 217 (1) (2006) 176–199.
- [16] T.P. Sapsis, A.J. Majda, Blended reduced subspace algorithms for uncertainty quantification of quadratic systems with a stable mean state, *Physica D* 258 (1) (2013) 61–76.
- [17] I. Hoteit, D.-T. Pham, G. Triantafyllou, G. Korres, A new approximate solution of the optimal nonlinear filter for data assimilation in meteorology and oceanography, *Mon. Weather Rev.* 136 (1) (2008) 317–334.
- [18] I. Hoteit, X. Luo, D.-T. Pham, Particle Kalman filtering: a nonlinear Bayesian framework for ensemble Kalman filters, *Mon. Weather Rev.* 140 (2012) 528–542.
- [19] A.J. Majda, D. Qi, T.P. Sapsis, Blended particle filters for large-dimensional chaotic dynamical systems, *Proc. Natl. Acad. Sci.* 111 (21) (2014) 7511–7516.
- [20] T.P. Sapsis, A.J. Majda, Blending modified gaussian closure and non-gaussian reduced subspace methods for turbulent dynamical systems, *J. Nonlinear Sci.* 23 (6) (2013) 1039–1071.
- [21] T.P. Sapsis, A.J. Majda, A statistically accurate modified quasilinear gaussian closure for uncertainty quantification in turbulent dynamical systems, *Physica D* 252 (1) (2013) 34–45.
- [22] Y. Lee, A.J. Majda, Multi-scale methods for data assimilation in turbulent systems, *Multiscale Model. Simul.* (submitted for publication).
- [23] I. Grooms, Y. Lee, A.J. Majda, Ensemble Kalman filters for dynamical systems with unresolved turbulence, *J. Comput. Phys.* 273 (2014) 435–452.
- [24] J.S. Liu, R. Chen, Sequential monte carlo methods for dynamic systems, *J. Amer. Statist. Assoc.* 93 (443) (1998) 1032–1044.
- [25] H.W. Sorenson, D.L. Alspach, Recursive Bayesian estimation using gaussian sums, *Automatica* 7 (4) (1971) 465–479.
- [26] A.J. Majda, J. Harlim, *Filtering Complex Turbulent Systems*, Cambridge University Press, 2012.
- [27] A. Majda, X. Wang, *Nonlinear Dynamics and Statistical Theories for Basic Geophysical Flows*, Cambridge University Press, 2006.
- [28] A. Majda, *Introduction to PDEs and Waves for the Atmosphere and Ocean*, Vol. 9, in: *Courant Lecture Notes*, American Mathematical Society, 2003.
- [29] N. Chen, A. Majda, D. Giannakis, Predicting the cloud patterns of the madden-julian oscillation through a low-order nonlinear stochastic model, *Geophys. Res. Lett.* 41 (15) (2014) 5612–5619.
- [30] T.P. Sapsis, P.F. Lermusiaux, Dynamically orthogonal field equations for continuous stochastic dynamical systems, *Physica D* 238 (23) (2009) 2347–2360.
- [31] E.S. Epstein, Stochastic dynamic prediction1, *Tellus* 21 (6) (1969) 739–759.
- [32] A.J. Majda, M. Branicki, Lessons in uncertainty quantification for turbulent dynamical systems, *Discrete Contin. Dyn. Syst.* 32 (9) (2012) 3133–3231.
- [33] E.N. Lorenz, Predictability: a problem partly solved, *Proc. Semin. Predict.* 1 (1) (1996) 1–18.
- [34] E.N. Lorenz, K.A. Emanuel, Optimal sites for supplementary weather observations: simulation with a small model, *J. Atmospheric Sci.* 55 (3) (1998) 399–414.
- [35] T.P. Sapsis, A.J. Majda, Statistically accurate low-order models for uncertainty quantification in turbulent dynamical systems, *Proc. Natl. Acad. Sci.* 110 (34) (2013) 13705–13710.